ATMOSPHERIC SCIENCE DIVISION

THE UNIVERSITY of TENNESSEE SPACE INSTITUTE

Tullahoma, Tennessee

Final Report
Prepared Under
Contract #NAS8-31718

J. R. Connell
Principal Investigator
Associate Professor, Atmospheric Science Division
The University of Tennessee Space Institute

for

George C. Marshall Space Flight Center
National Aeronautics and Space Administration

NUMERIC AND FLUID DYNAMIC REPRESENTATION OF TORNADIC DOUBLE VORTEX THUNDERSTORMS

by

Edward J. Marquart

Walter Frost

and

Wilson Boaz

May 1980

ABSTRACT

Current understanding of a double vortex thunderstorm involves a pair of contra-rotating vortices that exists in the dynamic updraft. The pair is believed to be a result of a blocking effect which may occur when a cylindrical thermal updraft of a thunderstorm protrudes into the upper level air and there is a large amount of vertical wind shear between the low level and upper level air layers.

Eagleman developed a numerical tornado prediction scheme based on the double vortex thunderstorm. The Energy-Shear Index (ESI) is part of the scheme and is calculated from radiosonde measurements. The ESI incorporates parameters representative of thermal instability and blocking effect, and indicates appropriate environments for which the development of double vortex thunderstorms is likely.

The ESI and modifications of it were tested using data derived from NASA's Fourth Atmospheric Variability Experiment (AVE IV). The results showed that the index has some general usefulness in forecasting tornadic outbreaks over a large area, but is probably not definitive enough for operational use. At times the results indicated large areas of expectant tornadic activity where little actually occurred. This deficiency led the author to investigate the possibility of incorporating into the index an additional dimensionless parameter to take into account the contribution to tornadic development associated with the fluid mechanics and shear instabilities of the double vortex thunderstorm itself.

To demonstrate the feasibility of obtaining information on this parameter, a wind tunnel investigation was conducted. The cylinder and jet in a laminar crossflow at conditions represented by a Reynolds number (based on cylinder diameter, crossflow velocity, and kinematic viscosity) near 5,000 were investigated. The method of investigation was flow visualization. Transition waves in the region extending from the cylinder to near three radii downstream of the cylinder's center were photographed.

Since complete simulation of the atmosphere with this wind tunnel facility is not possible, the results of the investigation cannot be directly related to a physical description of a double vortex thunderstorm. The direction for future investigation, however, is suggested from this study.

TABLE OF CONTENTS

LIST OF FIGURES

FIGURE PAGE

LIST OF SYMBOLS

AGL	Above ground level
AVE IV	Fourth Atmospheric Variability Experiment
°C	Degrees centigrade
cal	Calorie
cm	Centimeter
C_p	Specific heat capacity of dry air at constant pressure, 1.00 J/gm (°K)
D	Diameter of cylinder, 3.5 in.
EI	Energy Index
ESI	Energy-Shear Index
E_T	Total specific energy
f	Shedding frequency of von Karman vortex street
f_t	Shedding frequency of transition waves
gm	Gram
GMT	Greenwich mean time
h_{ASL}	Height of station in meters above sea level
J	Joule
°K	Degrees Kelvin
kg	Kilogram
km	Kilometer
L	Latent heat of vaporization (J/gm)
LCL	Lifting condensation level (meters)
L_o	Latent heat of vaporization at 0°C, 2,500 (J/gm)
m	Meter

mb	Millibar
q	Specific humdity (gm/kg)
Re	Reynolds number based on molecular viscosity
Re_t	Reynolds number based on turbulent eddy viscosity
S	Strouhal number
sec	Second
SI	Shear Index
T	Temperature
T_{DP}	Temperature dew point (°K)
T_{SFS}	Temperature at surface (°K)
V	Scalar velocity (m/sec or ft/sec)
W	Mixing ratio (gm/kg)
X	Distance measured in direction downstream of cylinder's center in units of cylinder radii
Y	Distance measured in cross stream direction from cylinder's center in units of cylinder radii
Z	Geopotential height (meters), (J sec^2/kg)
ν	Kinematic viscosity (ft^2/sec)
δ	Boundary layer height (inches)

CHAPTER I

NUMERIC AND FLUID DYNAMIC REPRESENTATION OF TORNADIC DOUBLE VORTEX THUNDERSTORMS

There are several methods by which to approach the problem of tornado prediction. One method is the use of a numerical prediction index, such as the one developed by Eagleman [1].[1]

Eagleman suggests that conditions necessary for the production of tornadic vortices depend on the development of a double vortex thunderstorm. Figure 1.1 is a schematic of the double vortex thunderstorm showing the relationship between the thermal updraft and the dynamic updraft. Current understanding of a double vortex thunderstorm involves a pair of contra-rotating vortices in the dynamic updraft which is believed to be the result of a blocking effect between the thermal updraft and the upper level air layers. A pair of contra-rotating vortices in a tornadic thunderstorm has been fairly well substantiated by dual-Doppler radar measurements [2].

The Eagleman model of a double vortex thunderstorm is the basis for a tornado prediction scheme that incorporates thermal instability (the Energy Index, EI) and a blocking effect (the Shear Index, SI). These two indices are combined when calculating the Energy-Shear Index (ESI). The Energy-Shear Index may be computed from data obtained from

---

[1] Numbers in brackets refer to similarly numbered references in the Bibliography.

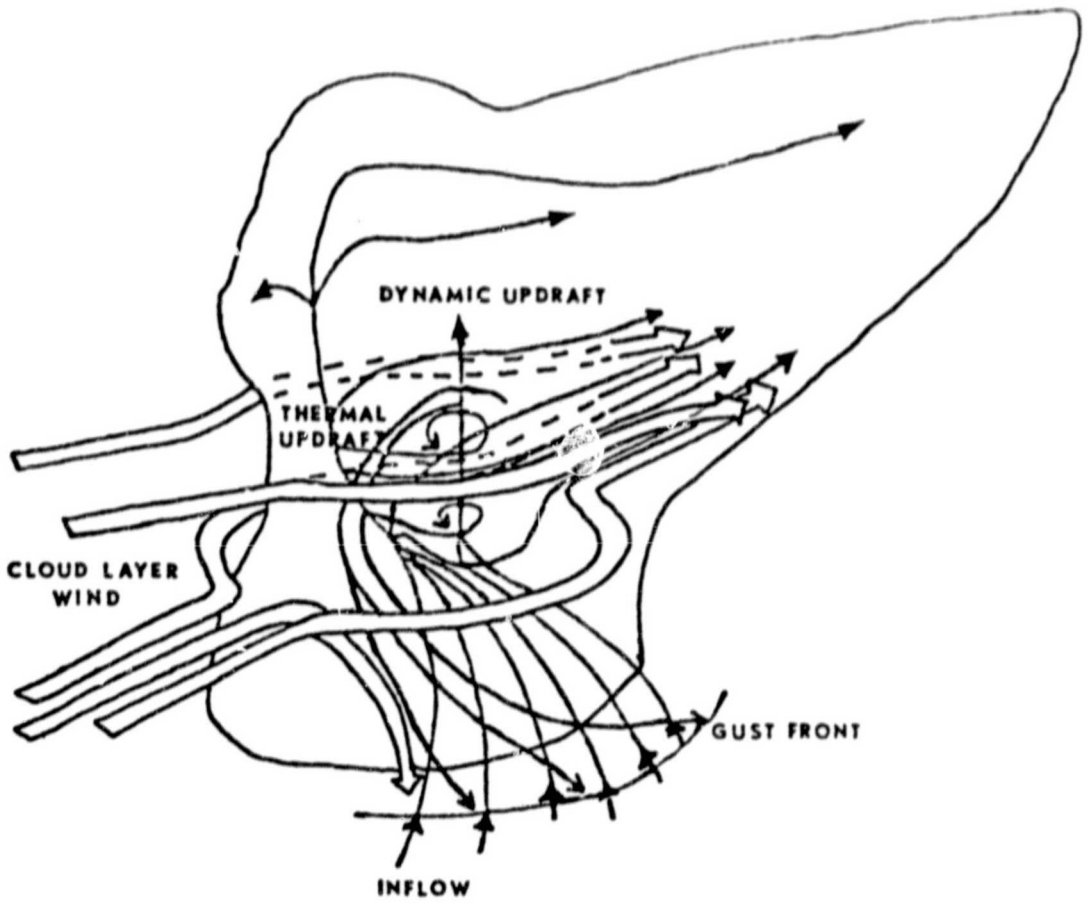

Figure 1.1. Schematic of the double vortex thunderstorm [5].

radiosonde measurements. It is indicative of appropriate environments for development of double vortex thunderstorms but it is not foolproof.

The present investigator tested Eagleman's model, and modifications of it, using data derived from NASA's Fourth Atmospheric Variability Experiment (AVE IV). NASA conducted the experiment on April 24-25, 1975 [3], in which 42 radiosonde stations participated.

I. THE ENERGY INDEX

The Energy Index, as developed by Darkow [4], reflects atmospheric instability. A measure of the instability of the atmosphere is the difference of total specific energy between the lower and upper level layers. The total specific energy of a unit air mass is the sum of the specific enthalpy, gravitational potential energy, latent heat, and kinetic energy,

$$E_T = (C_p\ T) + (g\ Z) + (L\ q) + (V^2/2)\ . \qquad (1.1)$$

Darkow explains that the kinetic energy term is usually two orders of magnitude smaller than the other terms. Due to the inaccuracy in reporting upper level humidity, the specific humidity (q) is found to be approximately equal to the mixing ratio (W). The latent heat of vaporization is assumed to be the value of 0°C.

Darkow compared average total specific energy profiles of environments near tornado touchdowns. The average total specific energy profile of 27 proximity soundings taken within 50 miles and 1 hour and 45 minutes of a tornado touchdown was obtained. Figure 1.2 shows the profile. The minimum total specific energy of soundings

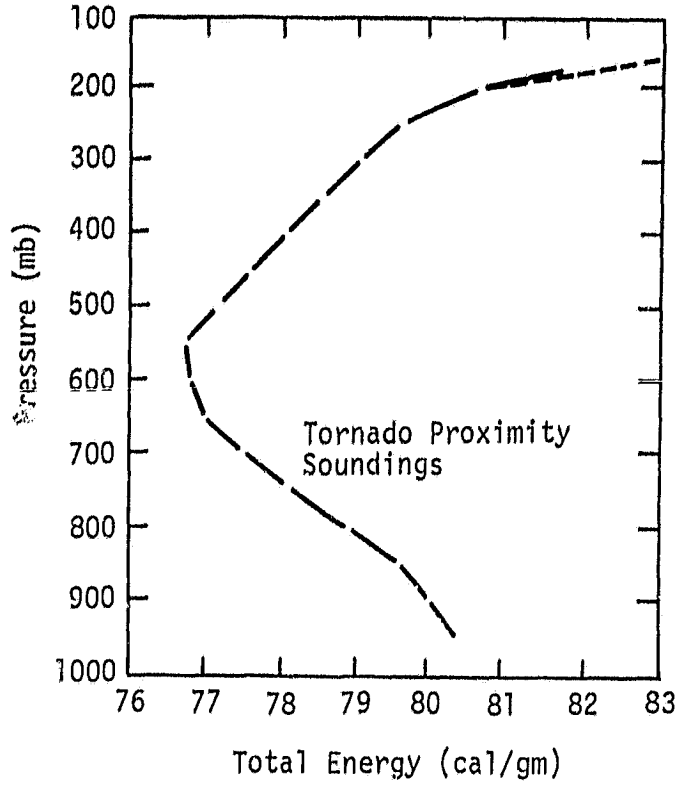

Figure 1.2. Average total specific energy profiles of 27 tornado proximity soundings [5].

taken in proximity of tornadoes occurs near the 500-mb pressure level. This fact was used as the basis for Darkow's Energy Index (EI).

The EI is defined as the difference in total specific energy between the 500- and 850-mb pressure level. The total specific energy of a pressure level is calculated by:

$$E_T = \left[T(°K) \times C_p(J/gm \ \ °K)\right] + \left[g(m/sec^2) \times z(m) \ \frac{1 \ kg}{1{,}000 \ gm}\right]$$

$$+ \left[L_o(J/gm) \times W(gm/kg) \ \ \frac{1 \ kg}{1{,}000 \ gm}\right]; \qquad (1.2)$$

$$E_T = T + 9.8 \ z \times 10^{-3} + 2.5 \ W \ . \qquad (1.3)$$

The Energy Index reflects instability, and when expressed in units of calorie per gram (cal/gm), is computed by:

$$EI = \frac{E_{T_{500}} - E_{T_{850}}}{4.18 \ (J/cal)} \ . \qquad (1.4)$$

The more negative the EI, the more the air mass is expected to be unstable. This is because low level air has more energy than upper level air.

II. THE SHEAR INDEX

The Shear Index (SI) was developed as an indicator of appropriate environment for the development of double vortex thunderstorms. Severe thunderstorms commonly travel considerably slower than the mean environmental wind. The intrusion of warm, moist air into upper level air and large amounts of vertical wind shear results in a

blocking effect. It was this concept of a blocking effect which led Eagleman to the development of a theoretical double vortex model of a tornadic thunderstorm.

The Shear Index reflects changes in wind velocities between low level and upper level layers. For a given storm velocity, the SI is the number of consecutive upper level layers, 150-mb-thick and taken every 50 mb, that have a component of velocity approximately equal to and opposing the average velocity of the low level wind. Figure 1.3 shows the relationship of the six upper level layers to the low level layer of the model. The average velocity of an upper level layer is computed using velocities measured 25-mb apart throughout the 150-mb-thick layer. The average velocity of the low level layer is computed using velocities taken 25-mb apart from the surface to the 850-mb level. Figure 1.4 shows the vector relationships of relative storm velocities and wind velocities.

Thunderstorm velocities have been observed to vary from 50 to 80 percent in magnitude and 60 deg in direction either side of the average cloud layer wind. Figure 1.5 shows 182 trail storm velocities 60 deg either side and 50 to 80 percent of the average cloud layer velocity. The trail storm velocity of 30 deg left and 55 percent of the average cloud layer wind is indicated on Figure 1.5. Shear Indexes are calculated for each of the 182 trail storm velocities. The velocity for which the maximum SI is calculated is the presumed real storm velocity. The average cloud layer velocity used in the calculation is the average of the velocities at the 850-, 700-, 500-, and 300-mb pressure levels. The greater the SI, the greater is the expected potential for double vortex formation in thunderstorms.

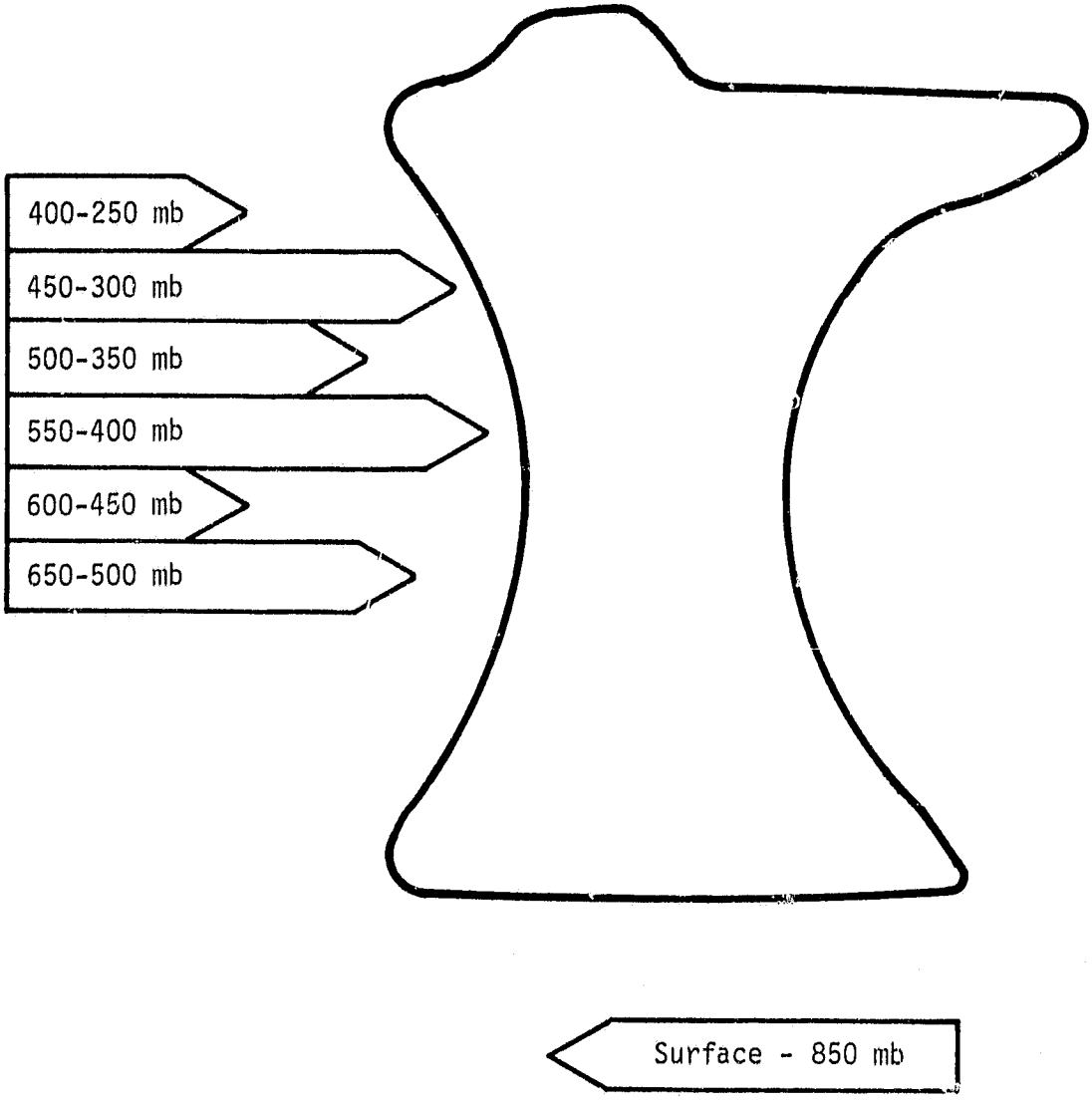

Figure 1.3. Relation of six upper level layers and the low level layer [5].

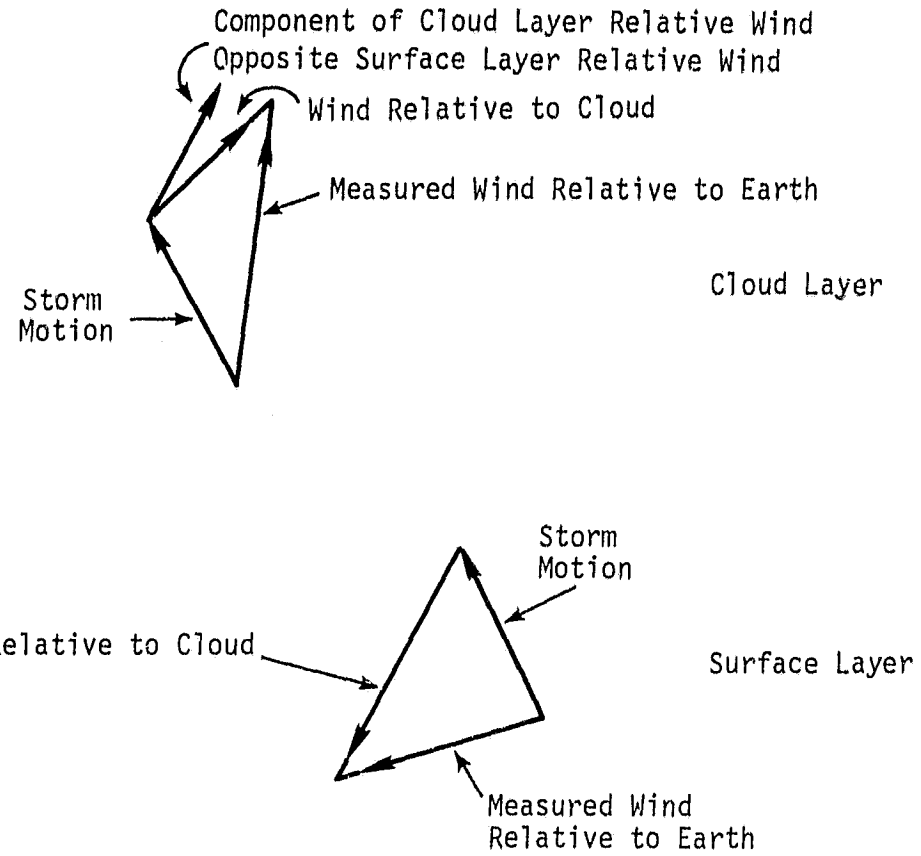

Figure 1.4. Vector relations of storm velocity and wind velocities [5].

Figure 1.5. One hundred and eighty-two trail storm velocities.

III. THE ENERGY-SHEAR INDEX

To account for thermal instability and environmental winds the Energy-Shear Index (ESI) incorporates the SI and EI. The ESI is the best empirical linear combination of the SI and EI based on a study of 59 soundings associated with tornadoes [1]. A proximity sounding is a sounding in the warm air ahead of a cloud front less than 120 miles from and within two hours before or one-half hour after a confirmed tornado touchdown. A non-proximity sounding is for the same time period but more than 200 miles away from a tornado. A precedence sounding is one that is greater than 200 miles away from a tornado and less than two hours before or one-half hour after a confirmed tornado touchdown. Figure 1.6 displays the 59 soundings and the line of best separation between proximity and non-proximity soundings.

The equation for this line is:

$$EI = 1/2\ SI - 2 \tag{1.5}$$

or

$$2\ EI - SI + 4 = 0\ . \tag{1.6}$$

The ESI is calculated by:

$$ESI = 4 - SI + 2\ EI\ . \tag{1.7}$$

When the ESI is negative, it represents conditions below the line of separation and double vortex thunderstorms are expected. For a more detailed explanation of the ESI, see Reference [1].

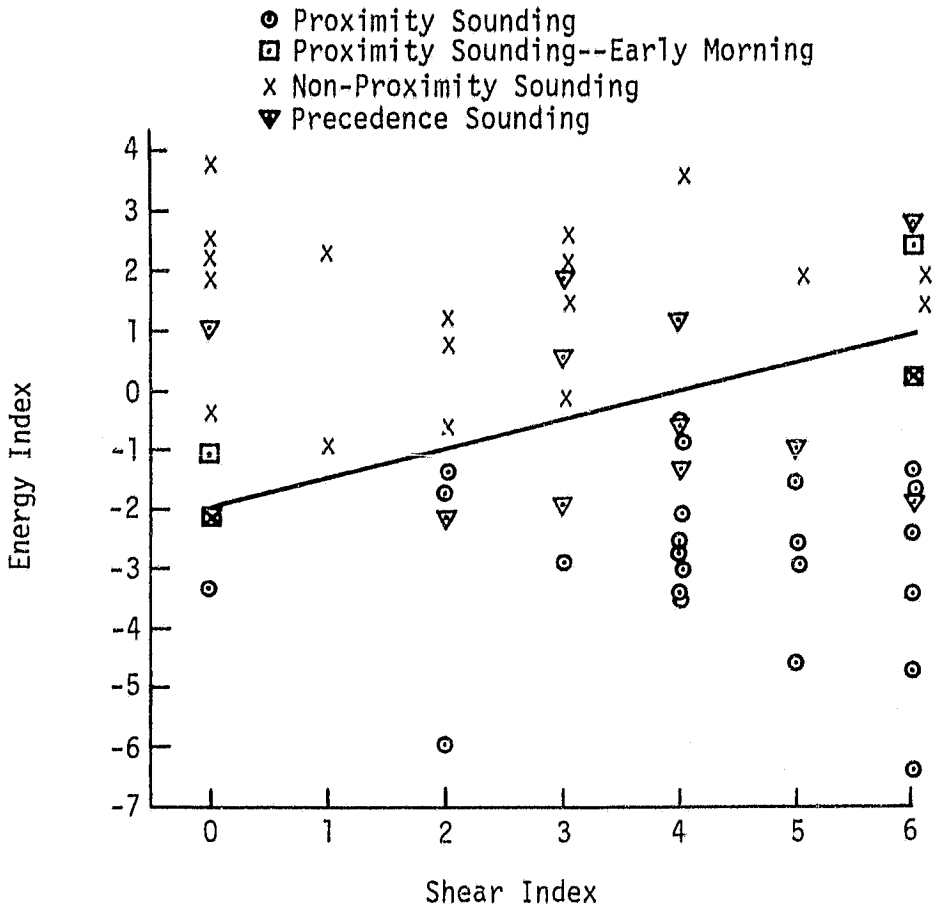

Figure 1.6. Scatter of EI and SI for 59 soundings and line of best separation [5].

Forecasting Ability

The forecasting ability of the Energy-Shear Index (see Appendix A) was tested by Ey [5] using data obtained during Nasa's Fourth Atmospheric Variability Experiment (AVE IV). The AVE IV experiment occurred 0:00 GMT April 24 to 12:00 GMT April 25, 1975. Forty-two weather stations in central and eastern United States participated. The synoptic conditions at the time of the experiment (by Ey [5]) are given in Appendix B. The severe events occurring during the experiment (by Turner [6]) are listed in Appendix C.

The results of Ey's test were deficient for operational use because large areas were predicted to have tornadic outbreak, yet little activity occurred. In an attempt to reduce the large area that falsely predicts tornadic outbreak ("false alarm" area) the present investigator modified and tested Eagleman's program (Program 1) three times.

Each modification of Eagleman's program was made to reduce the predicted "false alarm" area and expose layers which most affect the forecasting ability. The program was modified by altering the pressure levels used in obtaining the average wind velocity of the low level and the upper level air layers. Tests of the modifications were executed on The University of Tennessee IBM 360 computer by a program described in Reference [7].

The surface layer air is well mixed, resulting from interaction with the ground and extends up to the cloud base. There, it was concluded that a better representation of the low level layer velocity could be obtained by the average of velocities from the surface to the lifting condensation level.

The first modification (Program 2) obtains the low level wind from the average of the winds from the surface to the lifting condensation level, in 25-mb increments. For a dry adiabatic lapse rate of 10°K/km, the lifting condensation level was calculated by:

$$LCL(m) = \left[T_{SFS} - T_{DP}(°K)\right] \times \frac{1\ (km)}{10\ (°K)} \frac{1{,}000\ (m)}{1.0\ (km)} + h_{ASL}(m) . \qquad (1.8)$$

The predicting ability of Program 2 was tested using AVE IV data and compared with the predicting ability of Eagleman's program (Program 1). The results of the test are shown in Figures 1.7, 1.8, and 1.9 for time periods 24 April 1800 GMT, 24 April 2400 GMT, and 26 April 0600 GMT, respectively. The -1.0 isopleth is the expected line of separation between tornadic and non-tornadic storms. This isopleth is shown on the figures for each program. The circled number of the program indicates the isopleth for that program. Generally, altering the program in this manner did not change the predicting ability. Station 213, located near the southeastern coast, for the time period 24 April 2400 GMT, was added to the number of stations expecting tornadic outbreak where none occurred. The modification of the program involving the low level air layer had little effect on forecasting.

A second modification was made to the program to reduce the false alarm area. The modification this time involved the number and location of upper air layers used when determining blocking potential. The number of upper air layers was increased from 6 to 12 layers. The location of the additional layers was chosen so as to reflect blocking at greater altitudes. The 150-mb-thick layers were started every

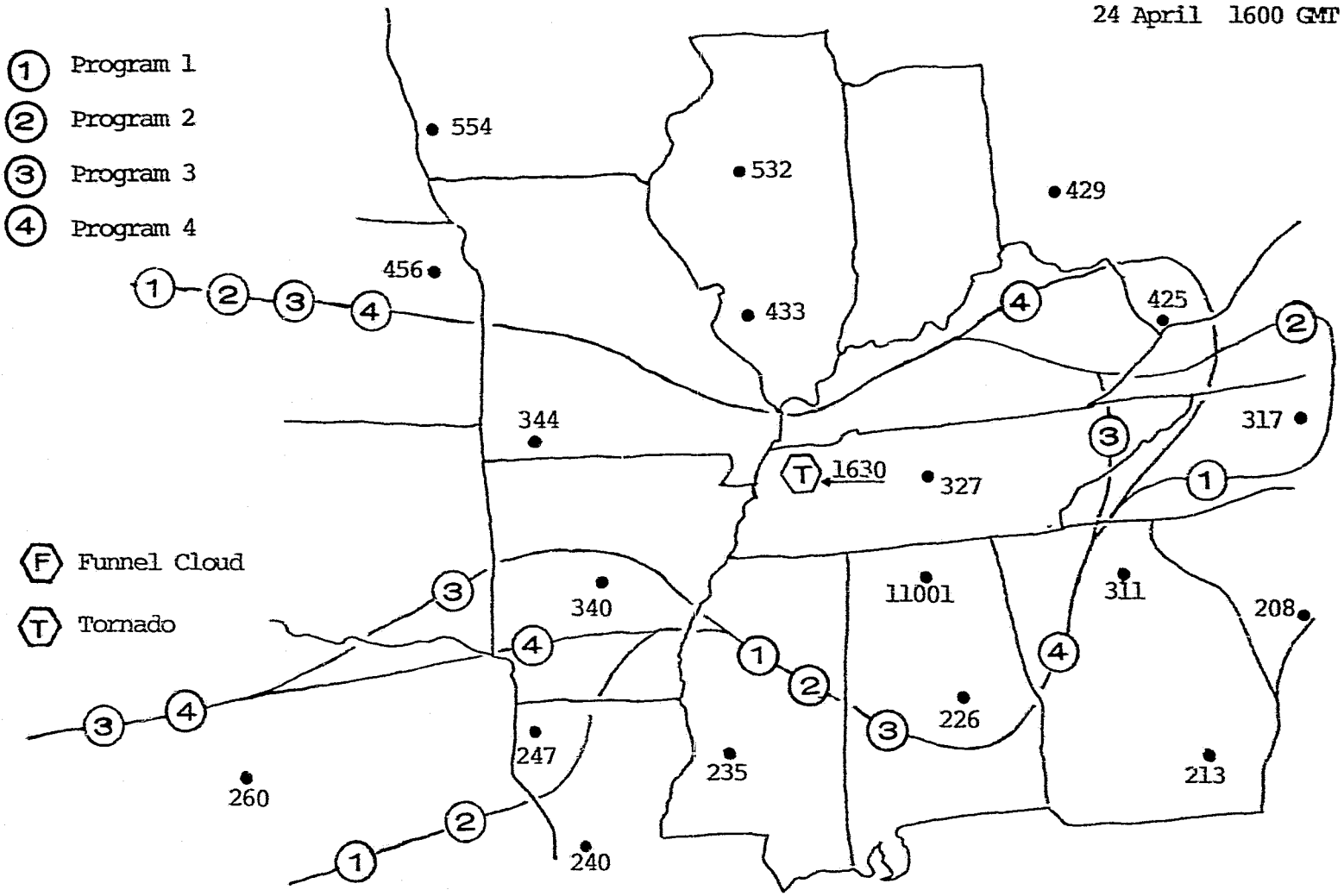

Figure 1.7. The 1.0 isopleth of programs for ESI, 24 April 1800 GMT.

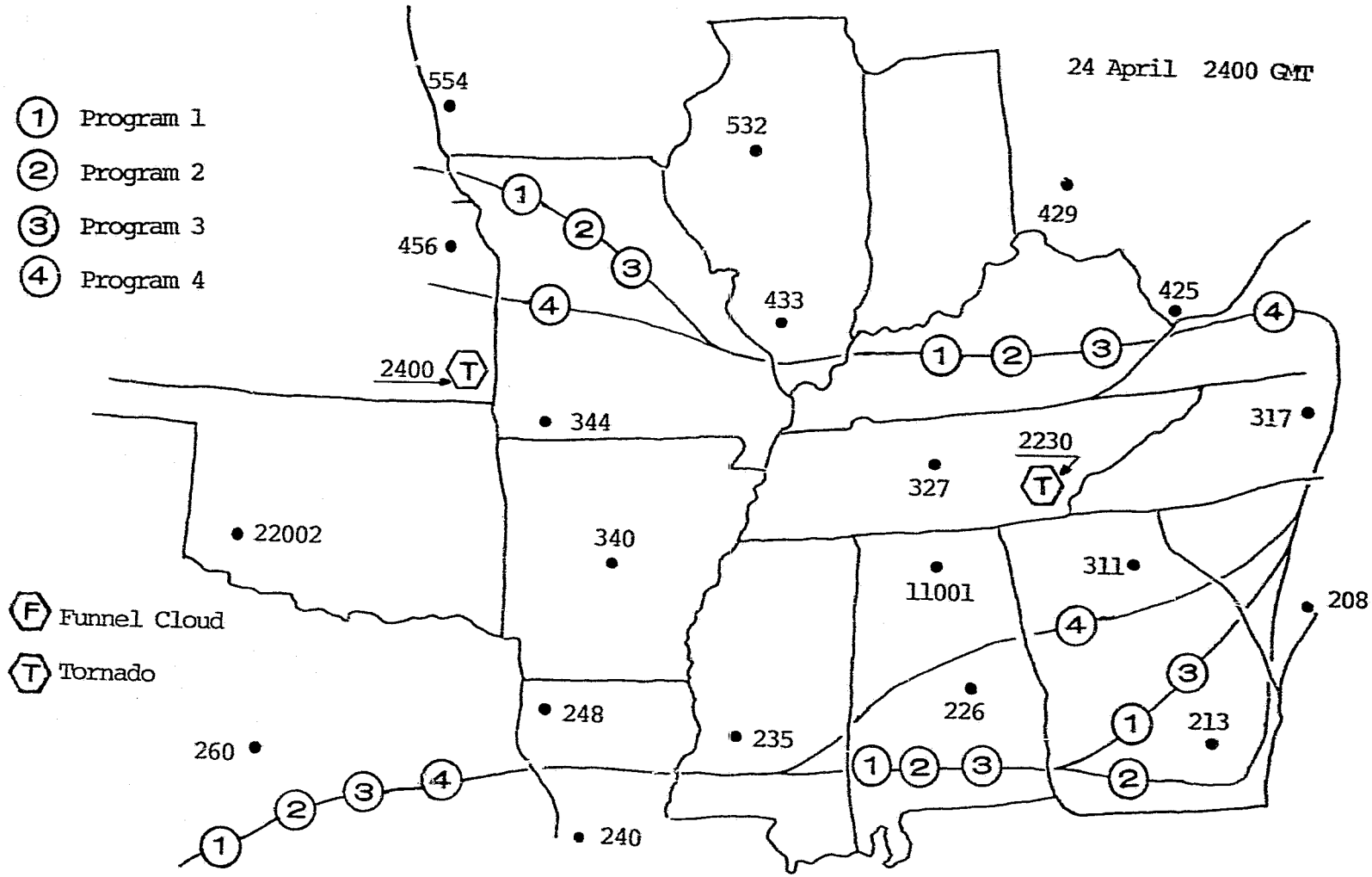

Figure 1.8. The -1.0 Isopleth of programs for ESI, 24 April 2400 GMT.

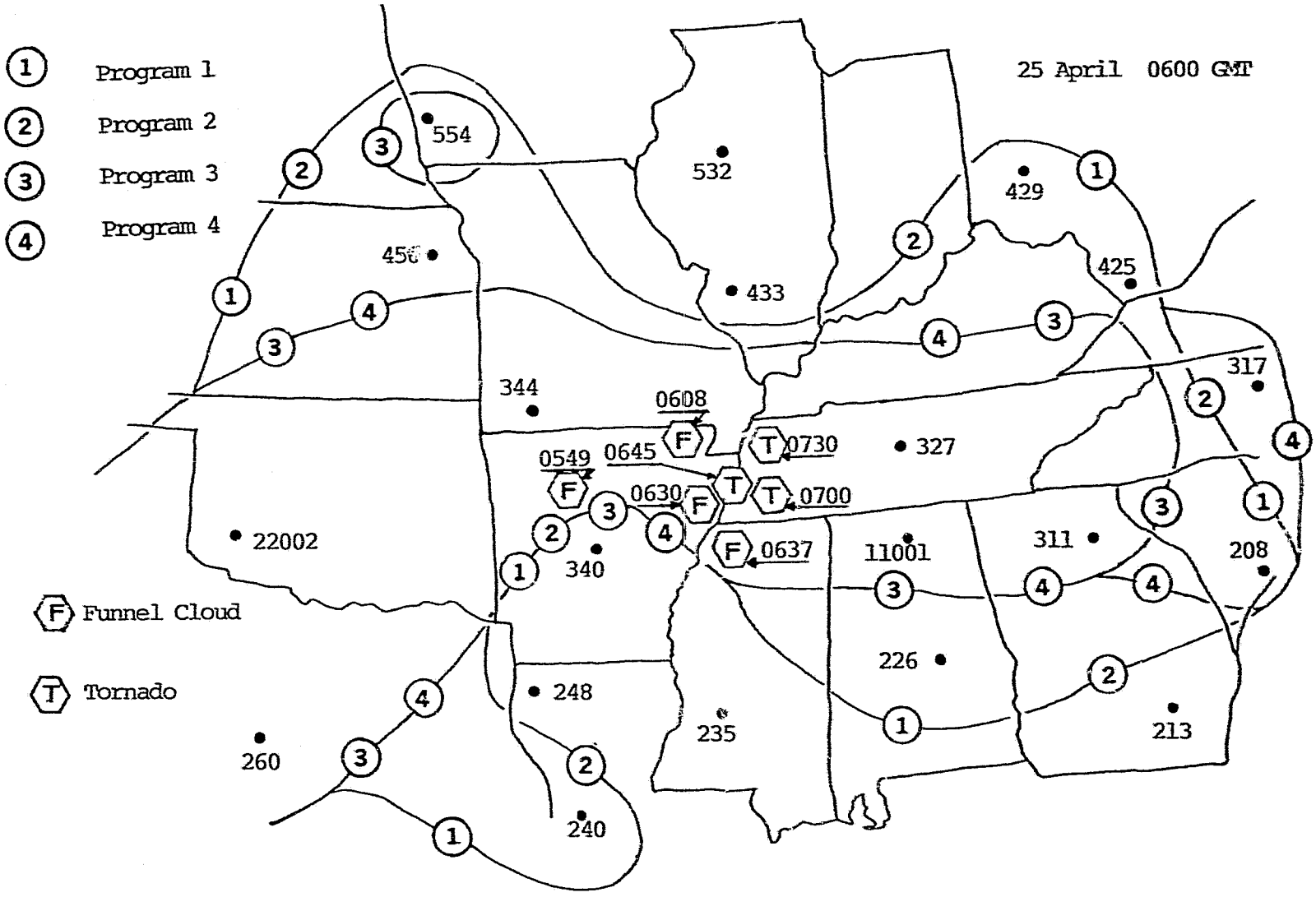

Figure 1.9. The -1.0 isopleth of programs for ESI, 25 April 0600 GMT.

50 mb and ranged from 800 to 250 mb. It was assumed, to maintain the same relative relationship of ESI among various programs, the SI obtained from Program 3 was divided by two. However, a weighted average may be more representative.

The forecasting ability of Program 3 was tested using the same AVE IV data. The results are shown in Figures 1.7, 1.8, and 1.9. The line with the circled 3 is the -1.0 isopleth obtained from Program 3. The figures show that some improvement was made for all three time periods. Figure 1.7 shows that for 24 April 1600 GMT improvement was made in eastern and south-central United States. Stations 260, 240, 340, and 317 were excluded from the false alarm area. Figure 1.8 shows that for 24 April 2400 GMT improvement was made in southeastern United States by eliminating Station 213. Figure 1.9 shows that for 25 April 0600 GMT improvement was made in northern and southern United States. Stations 240, 226, 208, 425, 429, and 456 were excluded from the false alarm area. A specific list of stations gained or eliminated is given in Table 1.1. The modification of the program involving the number and location of the upper level air layers had some beneficial effects.

To determine the importance of layers located between the lifting condensation level and the 800-mb level to blocking potential in double vortex thunderstorms, the upper level layers were shifted as a whole to begin at the lifting condensation level. The third modification (Program 4) used 12 layers and each layer was 150-mb-thick. The first layer begins at the lifting condensation level and a new layer starts every 50 mb.

Table 1.1. Comparison of Results Obtained from the Various Programs

	Stations Eliminated	Stations Gained
Program 2		
1800 GMT 24 April		213
2400 GMT 24 April		
0600 GMT 25 April		
Program 3		
1800 GMT 24 April	260 248 340 317	
2400 GMT 24 April	213	
0600 GMT 25 April	240 226 208 425 429 456	
Program 4		
1800 GMT 24 April		340 425
2400 GMT 24 April	226 456	
0600 GMT 25 April		208 317

The forecasting ability of Program 4 was tested using the same AVE IV data. The results are shown in Figures 1.7, 1.8, and 1.9 by the line with the circled 4. Figure 1.7 shows that for 24 April 1800 GMT Stations 340 and 425 were added to the false alarm areas that were located in northeast and central United States. Figure 1.8 shows that for 24 April 2400 GMT Stations 226 and 456 were eliminated in northwest and southeast United States. Figure 1.9 shows that Stations 208 and 317 were gained in the false alarm area in eastern United States. A specific list of stations gained and eliminated is given in Table 1.1. No significant increase or reduction in false alarm area was achieved by Program 4. The layers between the 800-mb level and lifting condensation level appear to have little effect on the forecasting ability of the ESI.

Summary of Predictor Approach

A program of Eagleman's model of a double vortex thunderstorm was modified three times. Each modification was to reduce the false alarm area and test the effect of forecasting ability of different layers in the double vortex thunderstorm. The forecasting ability of each modification was tested using the same AVE IV data. The results of each program were compared to the results of the previous program. The modification involving the low level layer showed little effect on forecasting ability. The modification involving additional upper level layers located at higher altitudes showed some beneficial effect on forecasting ability. The modification involving layers at lower altitudes (i.e., layers between the lifting condensation level and the 800-mb level) showed little effect on forecasting ability. The results

obtained during the sequence of tests that, modifications to Eagleman's tornado prediction program involving upper level layers at higher altitudes, had the greatest beneficial effect on forecasting ability. However, the results obtained are still deficient for operational use.

As a result of the deficiencies of these various programs in predicting tornadic storms, the present investigator believes that an additional parameter should be incorporated into the index to account for other dynamical effects characteristic of double vortex thunderstorms. An identification of the parameter must come about through a better understanding of the fluid mechanics in double vortex thunderstorms.

CHAPTER II

FLUID DYNAMIC REPRESENTATION OF DOUBLE VORTEX THUNDERSTORMS

The numerical tornado prediction scheme, explained and tested in the previous chapter, is based on the double vortex thunderstorm. The present investigator believes the scheme is incomplete and suggests that an additional dimensionless parameter be incorporated into the Energy-Shear Index (ESI). This parameter should represent the fluid mechanics of blocking in double vortex thunderstorms and be a measure of the shear instability associated with tornadic development. The parameter could be used to indicate a triggering mechanism in double vortex thunderstorms. A triggering mechanism initiates tornadic development and is needed to realize the blocking potential. The large "false alarm" areas could be eliminated if stations in the area fail to indicate a proper triggering mechanism. The purpose of this chapter is to demonstrate the feasibility of obtaining information on this parameter by wind tunnel investigation.

Eagleman suggests that a thermal updraft of a double vortex thunderstorm blocks the upper level air layers as a cylindrical body [2]. The flow around a cylindrical body separates on each side of this body creating a shear region behind it. The resulting wake of a thermal updraft is known as the dynamic updraft. It is in this dynamic updraft that tornadoes are believed to be created [2].

Turbulence levels in and around cumulonimbus clouds are extremely large [8]. The blocking effect of a thermal updraft can be

simulated by a cylinder in the crossflow that has sufficiently large turbulence levels. The wake of the cylinder would be similar to dynamic updrafts in double vortex thunderstorms. The wake could be analyzed under laboratory controls and information on the above suggested parameter could be obtained. Turbulence levels required for complete similarity between atmospheric thermal updrafts in double vortex thunderstorms and laboratory flows about cylinders would be extremely difficult to create in a wind tunnel and are beyond the scope of this study. Instead, a wind tunnel investigation of a cylinder in laminar crossflow was conducted. The conditions created in the wind tunnel are represented by a Reynolds number (based on cylinder diameter, crossflow velocity, and kinematic viscosity) of 5,000. This is of equal value to a Reynolds number obtained from multiplying average storm diameter to average wind speed in storms and dividing by the amount of turbulent transport of vorticity measured by aircraft in and around cumulonimbus clouds. Alehsandrov [8] had made these aircraft measurements and obtained the value of:

$$Re_t = 2.0 \times 10^3 \text{ to } 1.0 \times 10^4 , \qquad (2.1)$$

where a turbulent eddy viscosity of 20 to 100 m^2/sec is used.

Although the above Reynolds numbers are similar in value, it should be remembered that one is based on kinematic viscosity, while the other is based on eddy viscosity. Consequently, the present investigator does not suggest that any dynamical similarity exists between the atmosphere and the tunnel conditions. However, it was strongly felt that an investigation of the dynamic behavior of vortex shedding mechanics and/or shear wave instability behind cylinders in

the crossflow could shed light on the mechanism of tornadic generation behind thermal updrafts. The concept to be described, however, is the important issue.

I. PREVIOUS INVESTIGATIONS

Previous investigations of the phenomenon associated with the blocking effects of cylinders in a laminar crossflow have revealed an alternating periodic vortex street behind the cylinder. The first pictures of the alternating periodic vortex street behind a cylinder were published in 1902 [9]. In 1911, von Karman presented his famous vortex street theory that explains a stable alternating row of vortices could exist in a street behind a cylinder [9]. All Reynolds numbers used in discussing the phenomenon observed and measured behind cylinders in wind or water tunnels are based on free-stream velocity, cylinder diameter, and kinematic viscosity.

The Reynolds number range of periodic vortex shedding behind a cylinder is divided by Rosko [9] into two distinct subranges. The two ranges are the stable range and the irregular range. The stable range is composed of stable laminar vortices in a street extending for long distances behind the cylinder. The irregular range is composed of vortices in a street behind the cylinder where turbulent velocity fluctuations accompany the periodic formation of vortices. The diffusion of vorticity in the irregular range is by turbulent transport. This transport causes the wake to approach isotropic turbulence 40 to 50 diameters downstream [9].

At conditions represented by a Reynolds number range of 40 to 150, the alternating periodic vortex street is in the stable laminar

range, and can be observed for long distances downstream. The laminar vortices are dissipated by molecular diffusion of vorticity only. The mechanism of laminar vortex production operates in a way that a Strouhal number increases with an increasing Reynolds number [9]. The Strouhal number represents the shedding frequency in non-dimensional form. Figure 2.1 depicts this relationship in a graph of Strouhal numbers versus Reynolds number [10].

The Reynolds number range of 150 to 300 is a transition region bridging the stable range and the irregular range. The Reynolds number range of greater than 300 to less than 3×10^5 represents the conditions of the irregular range. The vortex street for this range is associated with turbulent velocity fluctuations. The mechanism of turbulent vortex production operates shortly downstream of the cylinder and in a way that the Strouhal number remains clearly constant with increasing Reynolds number, as shown in Figure 2.1.

In a portion of the irregular range of the von Karman vortex street a laminar shear region exists behind the cylinder. The end of the laminar shear region is unstable and alternately rolls up when forming turbulent vortices that make up the von Karman vortex street [11]. This laminar region begins at the separation points on the cylinder and ends at total breakup associated with transition. The total breakup, at conditions represented by a Reynolds number in the range of 3,500 to 8,500, occurs at (0.7) to (1.4) diameters downstream from the separation points on the cylinder [12].

Bloor [13] noted transition waves occurring in the laminar shear region behind the cylinder. The shear region consists of laminar

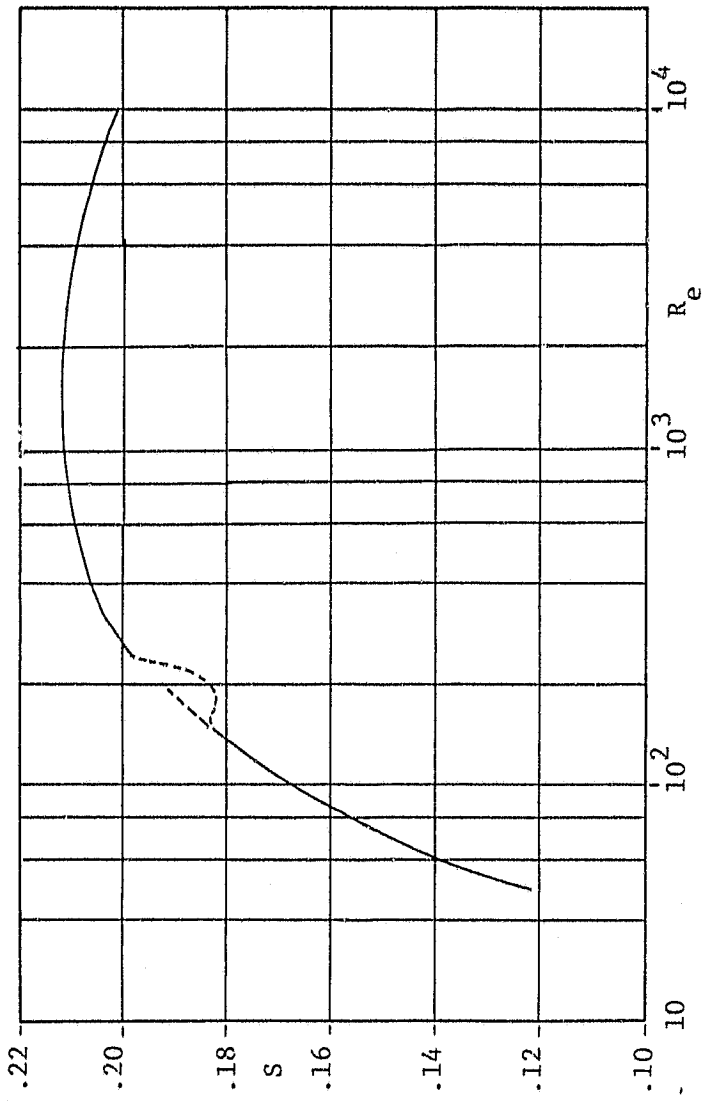

Figure 2.1. Strouhal number vs Reynolds number for a circular cylinder [9].

separated boundary layers. These waves precede the total breakup to turbulence and are believed by Bloor [13] to be two-dimensional, Tollmien-Schlichting waves caused by the instability in the separated boundary layers. Bloor has measured the frequency of wave production at conditions represented by a Reynolds number in the range of 500 to 50,000.

Gerrard [14] photographed these waves at conditions represented by a Reynolds number up to 2,000 by a flow visualization technique. Figure 2.2 is a drawing of his results. The linear portion of the transition waves can be seen to exist between three and somewhere near five radii downstream of the cylinder's center. Beyond this, the breakup to turbulence and the periodic formation of vortices that make up the von Karman vortex street exist.

Gerrard's flow visualization technique allowed transition waves to be photographed at a Reynolds number up to 2,000. To investigate transition waves by a flow visualization technique at conditions represented by a Reynolds number greater than 2,000, a wind tunnel was constructed.

II. CONSTRUCTION METHOD

The wind tunnel was constructed in a 6-ft by 30-ft by 8-ft trailer. One-fourth-inch-thick corrugated center cardboard formed the wind tunnel test section and the inlet nozzle. Three-inch-wide masking tape was used to fasten the cardboard edges together. Two layers of 1/16-in. mesh screen covered the opening of the inlet nozzle. The wind tunnel has a contraction ratio of 5.5, and its dimensions are shown in Figure 2.3.

Figure 2.2. Cylinder in Crossflow, Re = 2,000.

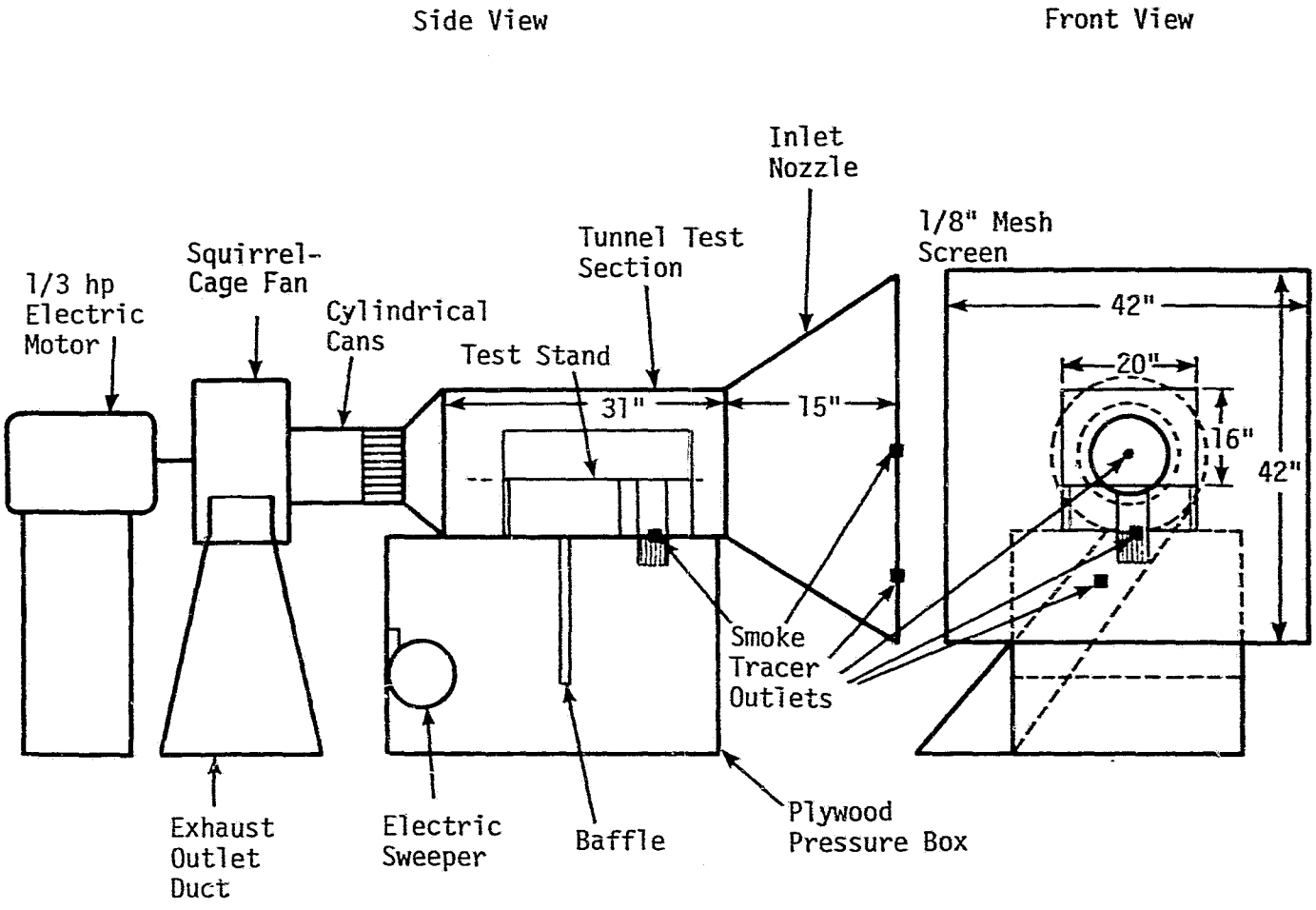

Figure 2.3. Sketch of wind tunnel.

A 1/3-hp electric motor was used to turn a squirrel-cage fan at the opposite end from the inlet nozzle. The fan sucked air through the tunnel and expelled it to the outside. Materials were needed to insure the straightness of airflow. Incorporated into the tunnel design were eight 3-in. by 6-in. aluminum cans. The ends of the cans were removed with a hacksaw so that they resembled a tubular structure. The cans were positioned immediately upstream of the squirrel-cage fan. In order to produce a honeycomb-like structure, experience indicated that straws produce the closest approximation. Therefore, upstream of the aluminum cans was composed of 1/4-in.-diam plastic soda straws, 1.5 in. in length. Held into place by two 1/16-in. mesh screens on each side, the straws were stacked to resemble a honeycomb. The test section is painted black with white lines in a square grid.

In order to view the test section, clear glass windows were incorporated in the tunnel design. Windows (21 in. by 16 in.) were positioned on the side and top of the test section. It was desirable to observe the test section from both the side and top views simultaneously. Consequently, a 24-in. by 18-in. mirror was placed over the glass on the top of the test section at a 45-deg angle from the horizontal plane. It provided a simultaneous view from the side and an inverted top view.

A titanium tetrachloride smoke generation system was developed. The system combines the use of a smoke gun and a fish tank air pump. White, neutrally buoyant smoke was pumped from the smoke gun through a 3/16-in.-diam plastic tube. At the end of the plastic tube is the

injection nozzle. The nozzle was made from a 0.02-in.-ID stainless steel tube.

Two slide projectors were used to illuminate the test section. An Olympus OM-1 35-mm single-lens reflex camera was positioned at the side of the test section such that the field of view included the simultaneous inverted top and side view.

Flow visualization techniques require wind tunnels with extremely low turbulence levels. Extreme care was taken to reduce these turbulence levels. The tunnel is located in one end of a 6-ft by 30-ft by 8-ft trailer. A wall divides the trailer into two sections. The section containing the tunnel consists of approximately one-third of the trailer's volume and is sealed off from the outside air. The dividing wall contains a door with a 3-ft by 3-ft section removed. Two 1/16-in. mesh screens, 1 in. apart, cover the removed section. This allows low turbulence air to enter the portion of the trailer that contains the tunnel. A door that opens to the outside air is located in the remaining two-thirds of the trailer. Since the air that flows through the tunnel is expelled to the outside during testing, this door was opened slightly to allow air to enter the trailer.

Initially, a velocity of 2.8 ft/sec (±0.2 ft/sec) was measured by a constant temperature hot-wire anemometer throughout the test section. The smoke was injected in the flow at the center of the beginning of contraction of the tunnel's inlet nozzle. Figure 2.4 is a photograph of smoke along the central streamline of the test section. The shutter speed is 1/60 sec. The straightness and sharp definition of the smoke line is evidence that the test section is laminar and in a steady state.

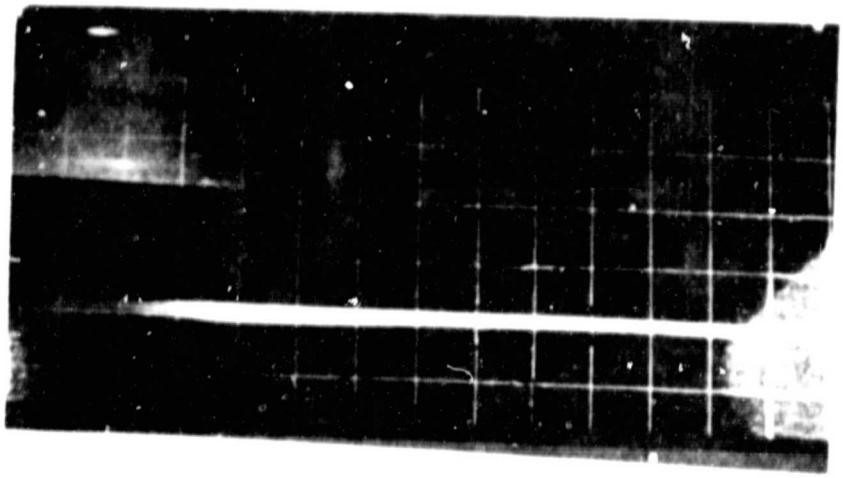

a. Top View

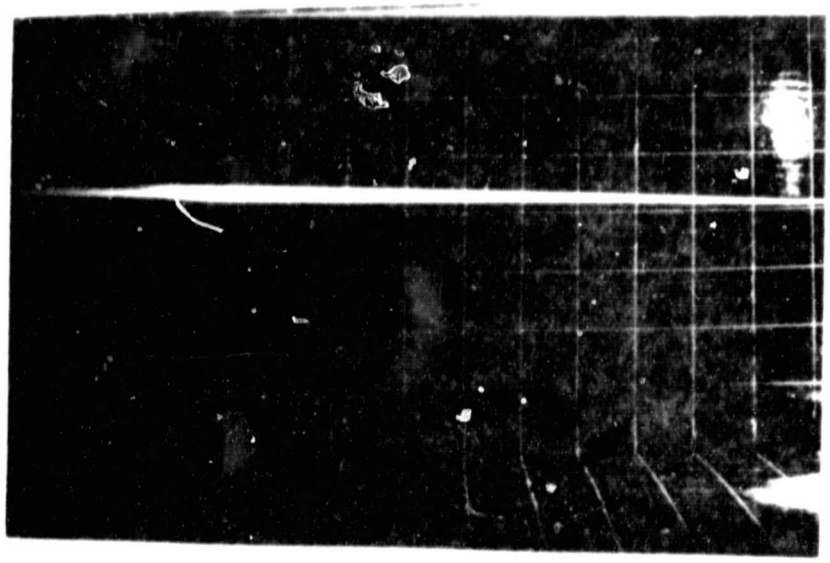

b. Side View

Figure 2.4. Photograph of center streamline of tunnel (shutter speed 1/60 sec).

A test stand that allows the testing of an air jet and a cylinder in crossflow was built. This stand and its dimensions are shown in Figure 2.5. The horizontal sheet of the test stand is 1/32-in. galvanized sheet metal. The sheet completely spanned the test section to divide it horizontally into an upper and a lower half. A 12-in. square section of the sheet metal directly behind the cylinder tube was removed and replaced with 1/8-in.-thick clear plexiglass in order that the lower half of the test section could be viewed from above. The sheet metal was held in the center of the test section by clear plexiglass sides.

The test stand is designed such that a cylinder is positioned in the lower half of the test section. The cylinder is a 3.5-in.-diam hollow cardboard tube. The tube has a 1/4-in. wall thickness and is assumed to be round to within 0.02 in. The surface of the tube is as smooth as paper and is painted black. Plastic straws (1.5-in.-long by 1/4-in.-diam) are placed in the bottom of the tube to resemble honeycomb. When the test stand is mounted in the test section, an air jet of varying speeds may be expelled through the tube into the upper half of the test section. When the tunnel test stand is installed in the test section, the flow in the test section is measured by a constant temperature hot-wire anemometer throughout the section to be 3.0 ft/sec ±0.2 ft/sec.

The Reynolds number representing the conditions of flow about the cylinder at the test conditions is computed by:

$$Re = \frac{V \times D}{\nu} = 5{,}468 \ , \qquad (2.2)$$

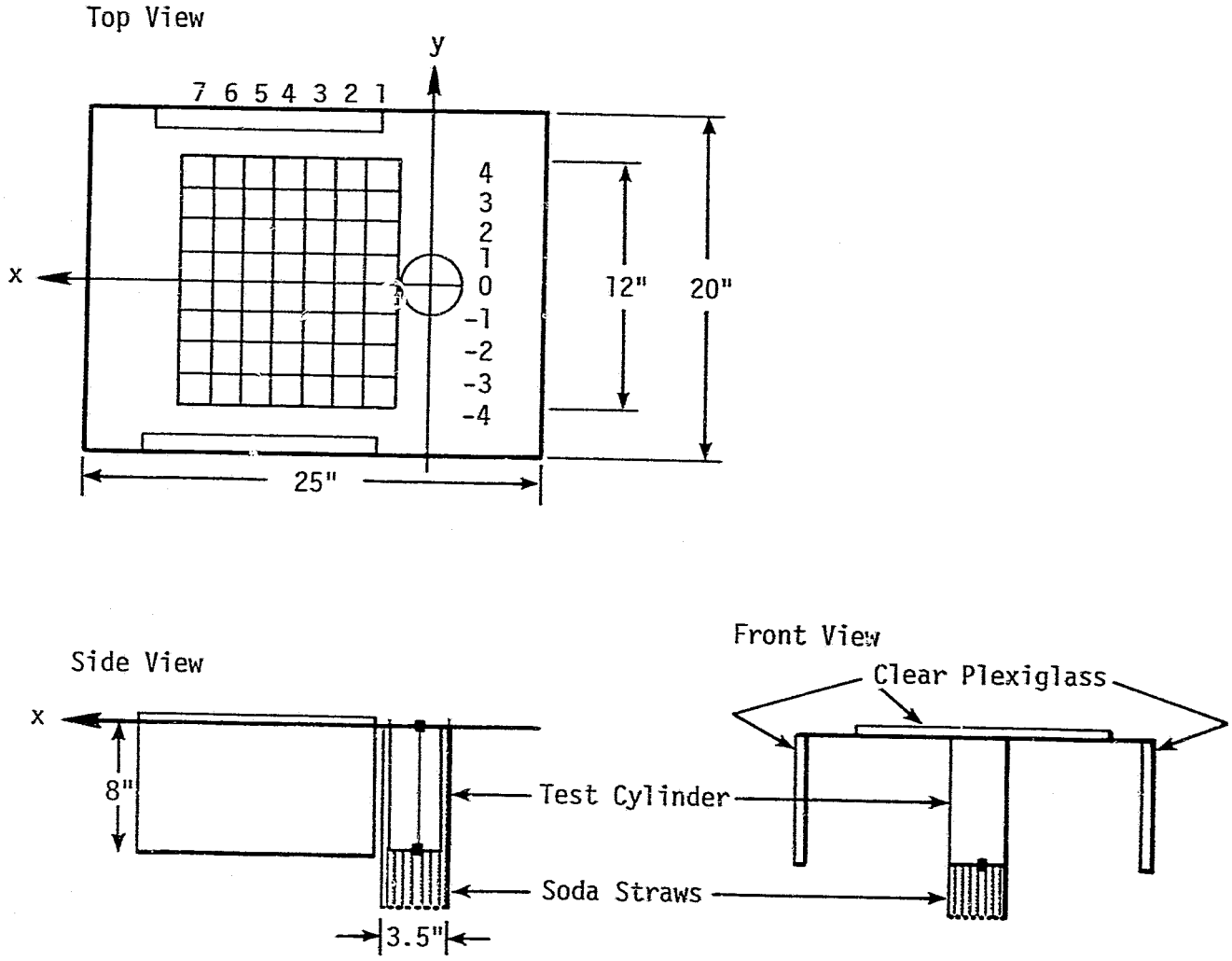

Figure 2.5. Sketch of test stand.

where

$$V = 3.0 \text{ ft/sec}, \; D = 3.5 \text{ in.}, \text{ and } \nu = 160 \times 10^{-6} \text{ ft}^2/\text{sec} .$$

The value of the kinematic viscosity is obtained from Schlichting [15]. The bottom end of the cylinder rests on the bottom of the test section. The boundary layer is assumed to remain small in the favorable pressure gradient created by the contraction of the tunnel's inlet nozzle. The cylinder is located 5 in. downstream of the end of the contraction of the tunnel inlet nozzle.

The horizontal section of the tunnel test stand holds the top of the cylinder in place and extends 5 in. upstream of the cylinder. The height of the laminar boundary layer on the test stand and tunnel wall at the location of the cylinder is calculated from [16]:

$$\delta = \frac{5.5}{\left(\frac{V_\infty}{\nu X}\right)^{1/2}} = 0.3 \text{ in.} \qquad (2.3)$$

The grid painted on the wall of the test section is one radius of the cylindrical tube that was incorporated in the design of the test stand. The distance X is measured in the downstream direction from the center of the cylinder, while Y is measured in the cross stream direction from the center of the cylinder. The origin of the grid is the center of the cylinder.

III. TEST PROCEDURE

To visually display the waves in the shear region behind the cylinder, smoke was introduced in the flow at the beginning of contraction of the tunnel's inlet nozzle. This was done so that the smoke line encountered the cylinder just off center of the front stagnation line on the cylinder. A photograph taken with a very short exposure time will display a smoke-filled laminar streakline as if it were stopped in time. Figure 2.6a is a photograph taken with the camera's shutter speed set at 1/60 sec. The field of view of the photograph extends over the range of X = 1 to 7.5 radii and of Y = 4.0 to -2.0 radii.

Due to its turbulent nature, evidence of the von Karman vortex production rate is not shown on film. However, the turbulent region past X = 3.0 radii was visually observed to oscillate near 22 times per 10 sec. This corresponds to a Strouhal number of 0.21, which is comparable to previous results by Roshko [9].

The prints shown in Figures 2.6a, b, c, and d were reproduced from slides and have in the process lost some of their sharpness. However, the definite sharpness of the smoke line indicates the smoke streakline up to 2.5 radii downstream of the cylinder's center is laminar. There is no problem in distinguishing the difference in sharpness levels before 2.5 radii and after 2.5 radii downstream of the cylinder's center.

The frequency of wave production was estimated by taking photographs at a variety of shutter speeds. Figures 2.6b, c, and d are photographs of the same region taken at camera shutter speeds of 1/30,

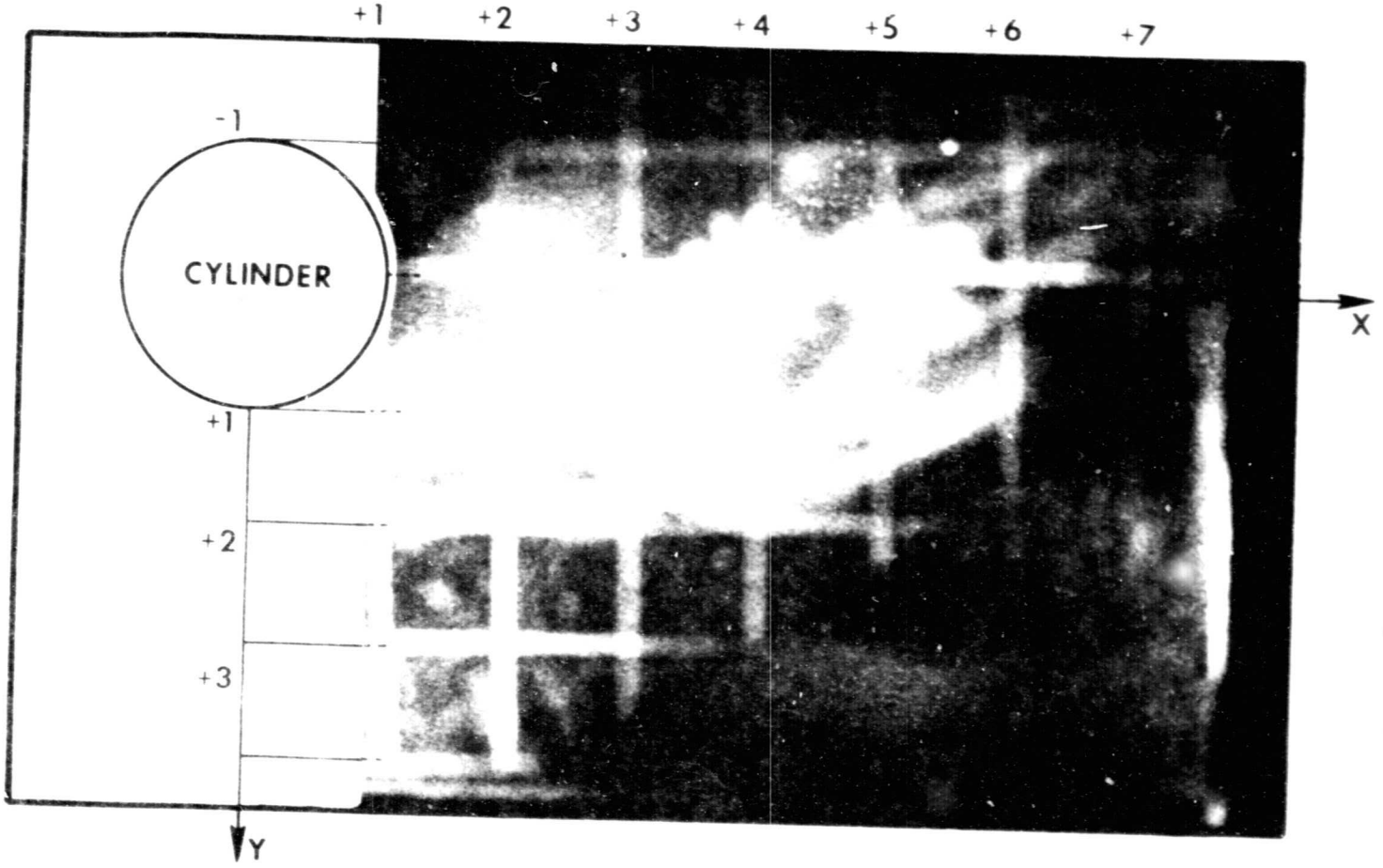

a. Shutter Speed 1/60 sec

Figure 2.6. Photograph of streakline next to the laminar wake behind the cylinder.

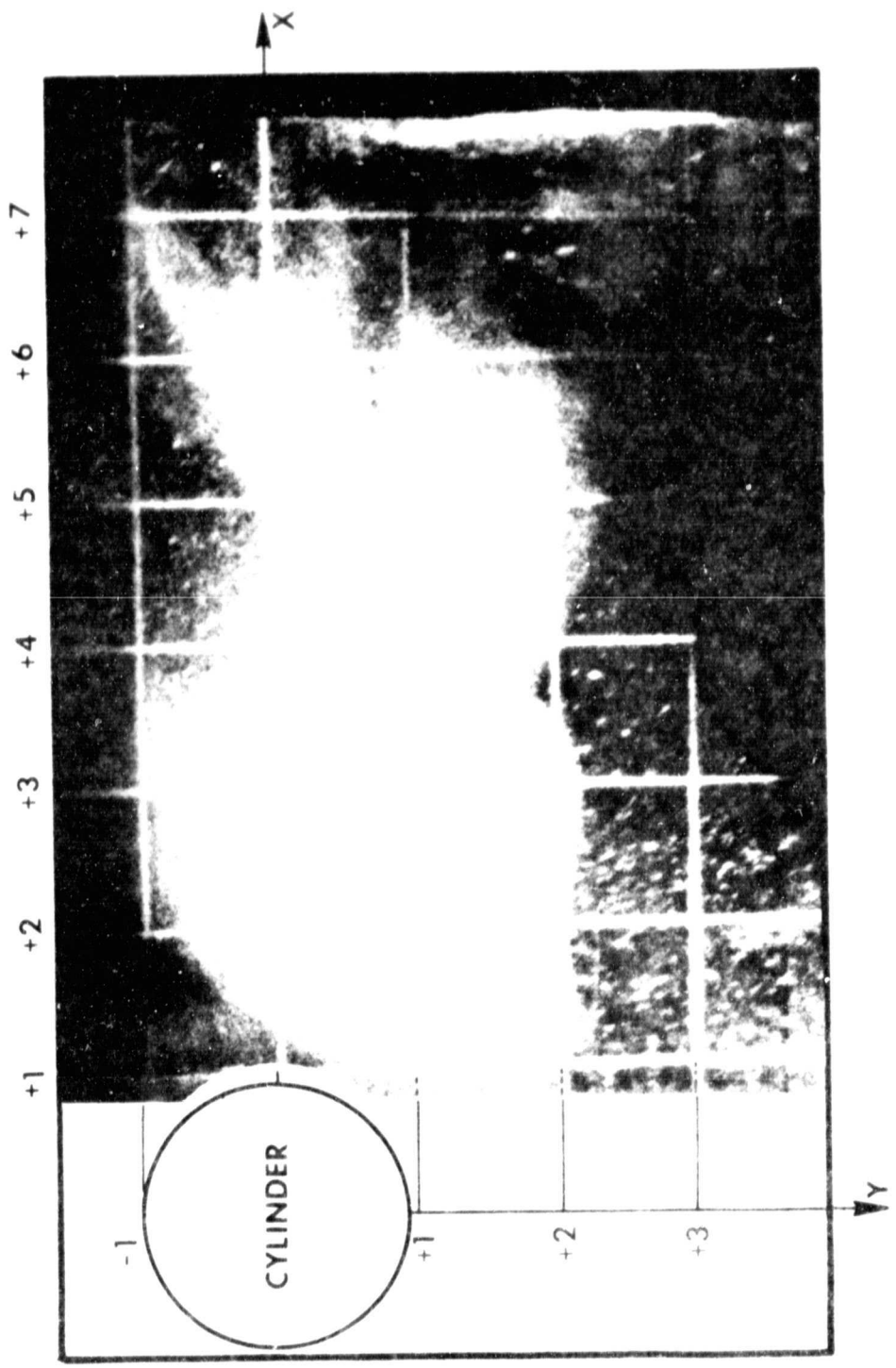

b. Shutter Speed 1/30 sec

Figure 2.6. (Continued)

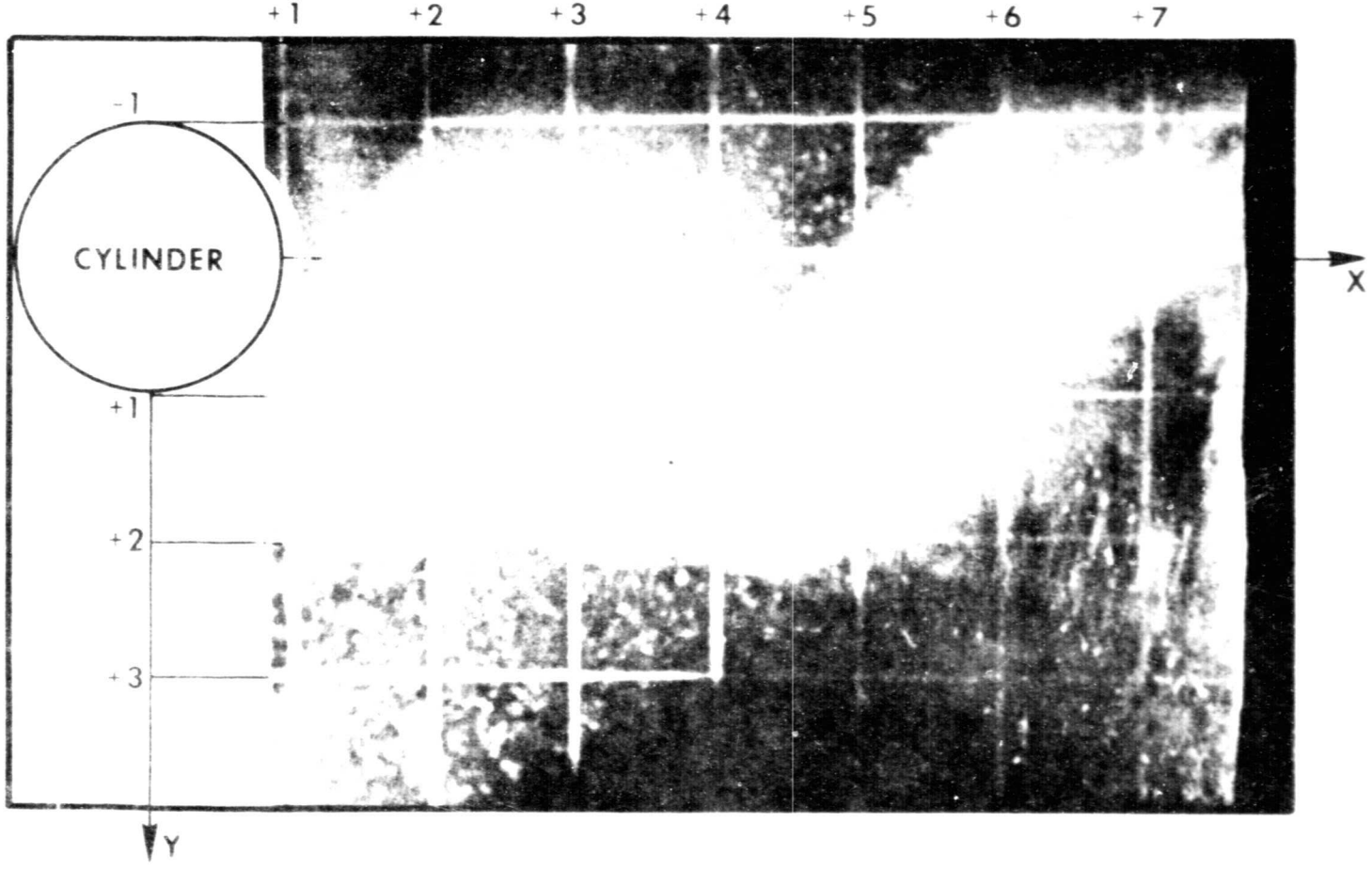

c. Shutter Speed 1/15 sec

Figure 2.6. (Continued)

d. Shutter Speed 1/8 sec

Figure 2.6. (Continued)

1/15, and 1/3 sec, respectively. Figure 2.6c shows movement of the wave on the smoke streakline making it less distinguishable than Figure 2.6b, while the wave in Figure 2.6d is completely indistinguishable. This indicates a wave production rate of greater than 8/sec and less than 15/sec. The ratio of wave production to von Karman vortex production is between 3.6 and 6.8. This estimated ratio compares well with measurements by Bloor [13]. The test results ratio and Bloor's measurements and ratio are shown in Figure 2.7.

The photographed waves in the laminar smoke streakline before 3.0 radii downstream of the cylinder's center, at conditions represented by a Reynolds number near 5,000, appear to be remarkably similar to the linear waves before 3.0 radii photographed by Gerrard. At conditions represented by a Reynolds number of 5,000, the breakup of turbulence appears to occur near 3.0 radii downstream of the cylinder's center. In Gerrard's photographs, at conditions represented by a Reynolds number of 2,000, the breakup to turbulence does not appear to occur until near 5.0 radii downstream of the cylinder's center. In the additional 2.0 radii that the laminar shear layers exist, at conditions represented by a Reynolds number of 2,000, the transition waves become non-linear and can be seen to have rolled up. At conditions represented by a Reynolds number near 5,000, the non-linear region, where transition waves roll up, could not be seen by the described flow visualization technique.

To see if the same trends occur in the wake behind an air jet directed normal to the flow, the same procedure was attempted. The wake behind the air jet was turbulent, however, and no smoke lines could be photographed.

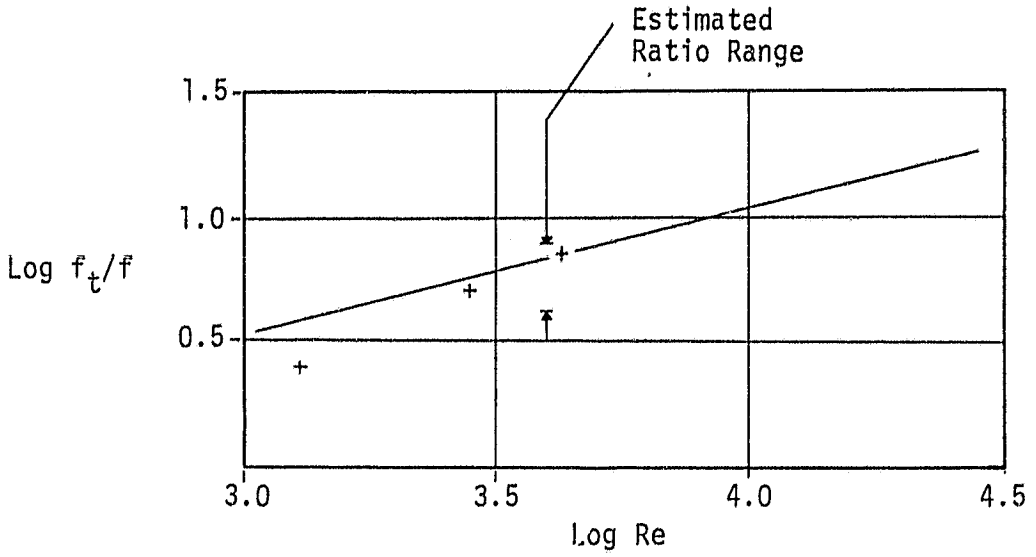

Figure 2.7. Ratio of transition wake production to von Karman vortex production vs Reynolds number [13].

IV. CONCLUSION

Although no relation can be drawn about the wake behind the tested cylinder and double vortex thunderstorms, the feasibility of obtaining information from a wind tunnel investigation was demonstrated. Further research is needed to develop a means of creating levels of turbulence in wind tunnels sufficiently large to guarantee similarity with natural conditions. If such a means can be created, then, the wakes of cylinders may be studied under laboratory controlled conditions. Information about the fluid mechanics in double vortex thunderstorms and instability associated with tornadic development can be obtained and incorporated into a dimensionless parameter. Such a dimensionless parameter could be incorporated into the Energy-Shear Index and improve the Index's ability to predict tornadic development.

BIBLIOGRAPHY

BIBLIOGRAPHY

1. Eagleman, J. R., Vincent M. Muirhead, and Nicholas Williams. Thunderstorms, Tornadoes and Building Damage. Lexington, Massachusetts: Lexington Books, 1975.

2. Eagleman, J. R., and Wes C. Lin. "Severe Thunderstorm Inertial Structure from Dual-Doppler Radar Measurements," Journal of Applied Meteorology, 16:1036-1048, October 1977.

3. Fucik, N. F., and R. E. Turner. "Data for NASA's AVE IV Experiment: 24-mb Sounding Data and Synoptic Charts," National Aeronautics and Space Administration TM X-64952, Space Sciences Laboratory, Marshall Space Flight Center, Huntsville, Alabama, August 1975.

4. Darkow, G. L. "The Total Energy Environment of Severe Storms," Journal of Applied Meteorology, 7(No. 2):199-205, July 1968.

5. Ey, L. "Wind Shear and Thermodynamic Weather Prediction on Indices Applied to the AVE IV Experiment." Unpublished Master's thesis, The University of Tennessee, Knoxville, 1978.

6. Connell, J. R., and L. Ey. "Wind Shear and Wet and Dry Thermodynamic Indices as Prediction of Thunderstorm Motion and Severity and Application to the AVE IV Experiment Data," National Aeronautics and Space Administration Report 150220, Redstone Arsenal, Huntsville, Alabama, March 1977.

7. Turner, R. E. "The Mechanics of Atmospheric Systems Derived Through Vertical and Horizontal Analysis of Parametric Data." Ph.D. dissertation, The University of Tennessee, Knoxville, 1976.

8. Aleksandrov, V. S., V. I. Silayeva, and S. M. Shmeter. "Atmospheric Turbulence in and Near Cumulonimbus Clouds," Tsentralnaya Aerologicheskaya Observatoriya Trudy 78:32-49, 1967. Air Force Cambridge Research Labs 69-0178, Trans. 45, L. G. Hanscom Field, Bedford, Massachusetts, April 1969.

9. Roshko, A. "On the Development of Turbulent Wakes from Vortex Streets," National Advisory Committee for Aeronautics TN-2913, [n.p.], 1953.

10. Roshko, A. "On the Drag and Shedding Frequency of Two-Dimensional Bluff Bodies," National Advisory Committee for Aeronautics TN-3169, [n.p.], 1967.

11. Fluid Motion Panel of the Aeronautical Research Committee. Modern Development in Fluid Dynamics. Vol. II. Edited by S. Goldstein. London: Oxford University Press, 1953.

12. Schiller, L., and W. Linke. "Druck-Und Reibungswiderstand des Zylinders bei Reynoldsschen Zahlen 5,000 bis 40,000," Zeitschrift für Fluglectnik und Motorluftschiffahrt, 24(No. 7):193-198, April 1933. English translation by National Technical Information Service, U.S. Department of Commerce, Springfield, Virginia. "Pressure and Frictional Resistance of a Cylinder at Reynolds Numbers 5,000 to 40,000," National Advisory Committee for Aeronautics TM-715, Washington, July 1933.

13. Bloor, Susan M. "The Transition to Turbulence in the Wake of a Circular Cylinder," Journal of Fluid Mechanics, 19:290-304, December 1964.

14. Gerrard, H. J. "The Wakes of Cylindrical Bluff Bodies at Low Reynolds Number," Philosophical Transactions of the Royal Society of London, 288:351-382, 1978.

15. Schlichting, H. Boundary Layer Theory. Toronto: McGraw-Hill Book Company, 1960.

APPENDICES

APPENDIX A

PROGRAM 4

```
$JOB          TIME=4,PAGES=99 ,NOLIST
C  THIS PROGRAM CALCULATES THE ENERGY-SHEAR INDEX FROM RAWINSONDE DATA
C     DATA IS READ FROM CARDS WITH THE FOLLOWING FORMAT
C   COLS 1-7 GEOPENTIAL HEIGHT, COLS 8-14 PRESSURE IN MB, 15-20 TEMPERATURE C
C    COLS 21-26 DEWPOINT TEMP,  C,  27-32 WIND DIRECTION, 33-37 WIND SPEED M/SEC
C  38-43 EASTWARD COMPONENT OF WIND, 44-49  NORTHWARD COMPONENT OF WIND
C  50-55 POTENTIAL TEMPERATURE, 56-61 EQUIVALENT POTENTIAL TEMPERATURE
C   COL 62-66 MIXING RATIO
C   COL 67-80 ARE USED FOR IDENTIFICATION
C
C   EACH DATA SET IS PRECEDED BY AN ID CARD WITH THE FORMAT
C  COL 1-5 STATION NUMBER,  6-33 STATION NAME, 34-35 DAY, 36-45 MONTH,
C   46-47 YEAR, 48-52 TIME OF DAY
C
C
C
C  DTEMP= DEWPOINT TEMPERATURE; TEMP= TEMPERATURE (DEG C); ET = TOTAL ENERGY OF
C  AN AIR PARCEL; WS = WIND SPEED AS MEASURED FROM THE SOUNDING; WD = WIND
C   DIRECTION AS MEASURED; ISTA = STATION NUMBER; GPHT = GEOPOTENTIAL HEIGHT IN
C  METERS; AMIXRA= MIXING RATIO (GM/KGM); EI = ENERGY INDEX
      DIMENSION DTEMP(3),DATE(5), PRESS(3),GPHT(3),TEMP(3),ET(2),WS(41)
      DIMENSION WD(41), DIRMID(12,200),SPDMID(12,200) ,RWS(40),RWD(40)
      DIMENSION CWS(40),MSS25(12,200),MSD25(12,200),SS25(12,200)
      DIMENSION SD25(12,200),ISAVE(12),DEV25(12,200)
      DIMENSION SRWS25(12,200),SRWD25(12,200)
      DIMENSION HEIGHT(25),PRESH(25)
      INTEGER HOUR
C
      DATA ALEFT/4HLEFT/
      DATA RIGHT/4HRGHT/
C
      COMMON TEMP, DTEMP, WD, WS, HOUR, NDAY, PRESS, GPHT
      COMMON ISTA
C   READ IN A DATA SET
C
  100 READ (5,1102) ISTA, DATE
      IF (ISTA .EQ. 99999) STOP
      READ (5,1104) GPHT(1), PRESS (1), TEMP (1), DTEMP(1), WD(1 ), WS(
     1 1),HOUR,NDAY
      DO 105 LOP1= 2,7
      READ(5,1103)HEIGHT(LOP1),PRESH(LOP1),WD(LOP1),   WS(LOP1)
  105 CONTINUE
      READ (5,1104) GPHT(2), PRESS (2), TEMP (2), DTEMP(2), WD(0 ), WS(
     1  0)
      HEIGHT(0)=0 PHT(2)
      PRESH(0)=PRESS(2)
      DO 110 LOP2= 9,21
      READ(5,1103)HEIGHT(LOP2),PRESH(LOP2),WD(LOP2),   WS(LOP2)
  110 CONTINUE
```

```
      READ (5,1104) GPHT(3), PRESS (3), TEMP (3), DTEMP(3), WD(22), WS(
     1 22)
      DO 115 LOP3= 23,41
      READ (5,1106) WD (LOP3), WS(LOP3)
  115   CONTINUE
 1102 FORMAT (15,20X,5A4)
 1103  FORMAT(2F7.1,12X,F6.1,F5.1)
 1104 FORMAT (2F7.1,3F6.1,F5.1,35X,I5,I3)
 1106 FORMAT (26X,F6.1,F5.1)
      WS=(TEMP(1)-DTEMP(1))/8.*1000.+GPHT(1)
C  IF DATA IS MISSING, PRINT MESSAGE
      IF (  GPHT(3) .EQ. 99.9 .OR. GPHT(3) .EQ. 99.9) GO TO 299
      IF (  TEMP(3) .EQ. 99.9 .OR. TEMP(3) .EQ. 99.9) GO TO 299
      IF ( DTEMP(2) .EQ. 99.9 .OR.DTEMP(3) .EQ. 99.9) GO TO 299
C
C*************************************************************************
C
C         CALCULATE THE ENERGY INDEX
C
      DO 240  I=2,3
        TEMPA = DTEMP (I) +273.16
        TEMPB =  TEMP (I) +273.16
        IF (TEMPA .LT. 273.16) GO TO 220
        EXP = (17.2693802 *(TEMPA-273.16))/(TEMPA-35.86)
        GO TO 230
  220 EXP = (21.874556*(TEMPA-273.16))/(TEMPA-7.66)
  230 E = 6.1078*(2.71828**EXP)
        AMIXRA = (622.*E)/(PRESS(I)-E)
      J=I-1
        ET(J) = .24*(TEMPB +2.5*AMIXRA+GPHT(I)/100.)
  240 CONTINUE
      EI= ET(2)-ET(1)
      GO TO 300
  299 WRITE (6,1012) DATE, ISTA
 1012 FORMAT (42HTHE ENERGY INDEX CANNOT BE CALCULATED FOR ,5A4,1X,I5)
      GO TO 100
C
C*************************************************************************
C
C  CALCULATE THE MEAN WIND VELOCITY OF THE CLOUD LAYER
C USING THE WINDS AT THE 850,700,500,& 300- MB LEVELS
C
  300 WRITE (6,1122) DATE, ISTA
 1122 FORMAT(////////,17X,5A4,1X,I5,40X,18HSHEAR INDEX VI MOD,//)
C  THIS LOOP TOTALS THE NUMBER OF 50-MB LEVELS THAT HAVE NO DATA AVAILABLE (ICI)
C  AND THE NUMBER OF LAYERS (USED TO CALCULATE THE AVERAGE) WHICH HAVE NO DATA
C  AVAILABLE(IFOUR)
      ICI= 0
      IFOUR = 0
      DO 304 I=1,20
        IM=I
        IF (I .NE. 1) IM=2*I-2
        IF (WS(IM).NE. 99.9) GO TO 304
        ICI= ICI+1
        IF (IM.EQ.8 .OR. IM.EQ.14 .OR. IM.EQ.22 .OR. IM.EQ.30) GO TO 302
        GO TO 304
  302 IFOUR = IFOUR+1
  304 CONTINUE
  306 N = 20-ICI
      XWIND =0.
      YWIND = 0.
C  THIS LOOP WILL SUM THE WINDS AT THE 850,700,500,& 300-MB LEVELS
C  DIVIDE BY THE NUMBER OF LAYERS TO OBTAIN THE AVERAGE, THEN FIND THE
C  MAGNITUDE(TMWS) AND DIRECTION (TMWD) IN DEGREES
      DO 312 J=1,20
        JM=J
```

```
      IF (J.NE. 1) JM=2*J-2
      IF (WS(JM) .EQ. 99.9) GO TO 312
      IF (JM.EQ.8 .OR. JM.EQ.14 .OR. JM.EQ.22 .OR. JM.EQ.30) GO TO 310
      GO TO 312
310   RADWS = WD(JM)/57.296
      XWIND = XWIND + WS(JM)*COS(RADWS)
      YWIND = YWIND + WS(JM)*SIN(RADWS)
312   CONTINUE
320 AVXW = XWIND/(4.-FLOAT(IFOUR))
    AVYW = YWIND/(4.-FLOAT(IFOUR))
    THWS= SQRT(AVXW**2 +AVYW**2)
    DD = AVYW/AVXW
    THWD = ATAN(DD)*57.296
C  FIND THE REAL VALUE OF THWD BY SELECTING THE PROPER QUADRANT
    IF(AVXW.GE.0.) GO TO 350
    THWD = THWD +180.
350 IF (THWD .LT. 0.) THWD = THWD+360.
    IF ( THWD .GT. 360.) THWD = THWD-360.
C  INITIALIZE VALUE OF ISAVE AND INDSHR
    DO 365 M=1,11
     ISAVE(M) =1
365  CONTINUE
    INDSHR = 0
    DO 699 III= 1,2
    DO 699 K = 1,61,5
    DO 699 L = 1,31,5
C  THE VALUE OF III DETERMINES WHETHER DEVIATION IS TO THE RIGHT OR LEFT OF THE
C  AVERAGE CLOUD LAYER WIND,K IS THE ANGLE OF DEVIATION.  L+50 IS THE
C  PERCENTAGE OF AVERAGE WIND SPEED
C
C
C**************************************************************************
C
C  CALCULATE RELATIVE WIND VELOCITIES BASED ON DEVIATIONS
C  OF STORM DIRECTIONS FROM THE MEAN WIND VELOCITY
C
    IHUNDR= 50+L-1
    IDEVIT = K-1
C  SS= TEST STORM SPEED;  SD= TEST STORM DIRECTION
    SS = THWS *FLOAT(50+L-1)/100.
    IF (III.EQ.1) DIR= RIGHT
    IF (III.EQ. 2) DIR= ALEFT
    IF ( DIR.EQ. ALEFT) IDEVIT= IDEVIT+5
    IF (III.EQ.2) GO TO 401
    SD= THWD +FLOAT(K)-1.
    GO TO 402
401 SD= THWD-FLOAT(K)-4.
402 DO 430 LL=1,20
      LLM = LL
      IF (LL.NE.1)LLM=2*LL-2
C  GAMMA = DIFFERENCE BETWEEN TEST STORM DIRECTION AND DIRECTION OF MEASURED
C  WIND;  RADGA = GAMMA IN RADIANS
      GAMMA =SD-WD(LLM)
      RADGA= GAMMA/57.296
C  RWS = RELATIVE WIND SPEED BETWEEN THE STORM AND THE MEASURED WIND
      RWS(LLM) = SQRT(WS(LLM)**2+SS**2-2.0*WS(LLM)*SS*COS(RADGA))
      SINSS =  (SS*SIN(RADGA))/RWS(LLM)
C. THIS SEGMENT PREVENTS THE GENERATION OF SINES OF VALUE LARGER THAN 1.0 IN
C  ABSOLUTE VALUE DUE TO ROUND OFF ERRORS IN THE COMPUTER
    NSIN =0
    IF (SINSS.LT.0.0) NSIN=1
    IF (ABS(SINSS).GE. .9999998 .AND. ABS(SINSS).LT.1.0001 ) SINSS=1.0
    IF (SINSS.GT.1.) GO TO 1234
    IF (NSIN .EQ.1 .AND. SINSS .EQ. 1.0) SINSS = -1.0
    IF ((1.0-ABS(SINSS)**2.) .GT. 0.0) GO TO 405
    WRITE(6,5302) III,K,L,LLM,SINSS,COSSS
```

```
      COSSS=0.0
      GO TO 410
  405  COSSS =SQRT(1.0- ABS(SINSS)**2.0)
 5302 FORMAT (4I4,2E14.6)
  410 IF (COSSS .LE. .000001) GO TO 415
        TANSS= SINSS/COSSS
        BETA = ATAN(TANSS)*57.296
      GO TO 420
  415 WRITE (6,5302) III,K,L,LLM,SINSS,COSSS
      IF (SINSS - 0.0) 416,416,417
  416 BETA = 270.
      GO TO 420
  417 BETA = 90.
  420   RWD(LLM) =WD (LLM)-BETA
        IF (RWD(LLM).LT.0.) RWD(LLM)= RWD(LLM)+360.
        IF (RWD(LLM).GT.360.) RWD(LLM)= RWD(LLM)-360.
  430   CONTINUE
C N IS THE NUMBER OF 50-MB LEVELS THAT HAVE DATA
C  CALCULATE THE AVERAGE RELATIVE WIND IN THE SURFACE-850MB LAYER)
      DO 435 IQ=2,10,2
      IQQ=IQ-1
      IIQ=IQQ+7
      IIIQ=IQQ+29
      IF(HEIGHT(IQ).GT.HQ) GO TO 437
435   CONTINUE
437   ILCL=IQQ/2+2
      IDI = 0
      DO440 M=1,ILCL
        MM=M
        IF (M.NE. 1) MM=2*M-2
        IF (WS(MM).NE. 99.9) GO TO 440
        IDI = IDI+1
  440   CONTINUE
      XSUM = 0.
      YSUM = 0.
      NN=ILCL-IDI
      DO 450 II=1,ILCL
        IIM=II
        IF ( II.NE.1) IIM= 2*II-2
        IF ( WS(IIM).EQ. 99.9) GO TO 450
        RRWD = RWD(IIM)/57.296
        XSUM= XSUM+RWS(IIM)*COS (RRWD)
        YSUM ='YSUM+RWS(IIM)*SIN(RRWD)
  450   CONTINUE
C
C*************************************************************************
C
C  CALCULATE LAYER AVERAGES
C
C  AVRWS AND AVRWD ARE THE AVERAGE RELATIVE WIND SPEED AND DIRECTION
C  RESPECTIVELY OF THIS LAYER
C  THIS PROGRAM SEGMENT CALCULATES THE SURFACE- 850-MB AVERAGE WIND SPEED AND
C DIRECTION
      AVXSUM = XSUM/FLOAT(NN)
      AVYSUM = YSUM/FLOAT(NN)
      AVRWS = SQRT( AVXSUM**2+AVYSUM**2)
      D = AVYSUM/AVXSUM
      AVRWD = ATAN(D)*57.296
      IF (AVXSUM.GE. 0.) GO TO 501
      AVRWD = AVRWD+180.
  501 IF ( AVRWD .LT. 0.) AVRWD = AVRWD+360.
      IF (AVRWD .GT. 360.) AVRWD = AVRWD-360.0
      CWD = AVRWD +180.
      IF ( CWD.GT. 360.) CWD = CWD-360.
      DO 570 KK=IIQ,IIIQ,2
       KKJ =0
```

```
      XRW =0.
      YRW = 0.
      KKI = KK-6
      KKK=KK
      DO 520 KKL= KKI,KKK,2
        IF (WS(KKL).EQ.99.9) GO TO 510
        RRRWD =RWD(KKL)/57.296
        XRW = XRW+RWS(KKL)*COS(RRRWD)
        YRW = YRW +RWS(KKL)*SIN(RRRWD)
        GO TO 520
  510   KKJ= KKJ+1
  520   CONTINUE
  525 IF (KKJ.EQ.4) GO TO 550
      XAVRW = XRW/(4.-FLOAT(KKJ))
      YAVRW = YRW/(4.-FLOAT(KKJ))
      XAVRWS = SQRT(XAVRW**2+ YAVRW**2)
      E= YAVRW/XAVRW
      XAVRWD = ATAN(E)*57.296
      IF ( XAVRW.GE.0.) GO TO 530
      XAVRWD = XAVRWD+180.
  530 IF (XAVRWD.LT.0.) XAVRWD = XAVRWD+360.
      IF ( XAVRWD.GT. 360.) XAVRWD = XAVRWD-360.
      CDEG1 = (CWD-XAVRWD)
     IF (CDEG1.GT.90.) GO TO 560
      CDEG2 = CDEG1 + 90.
      IF (CDEG2.LT.0.) GO TO 560
  540 CDEG = CDEG1/57.296
      CWS(KK) =XAVRWS*COS (CDEG)
      GO TO 570
  550 CWS(KK) =-1.
      GO TO 570
  560 XAVRWD = XAVRWD + 360.
      CDEG1 = XAVRWD-CWD
      XAVRWD = XAVRWD-360.
      IF (CDEG1.LT. 90.) GO TO 540
      CWD = CWD +360.
      CDEG1 = CWD -XAVRWD
      CWD = CWD-360.
      IF (CDEG1 .LT. 90.) GO TO 540
      CWS (KK)= -1.
  570 CONTINUE
     YMID =0.
     XMID =0.
     JJJJ=0
C  THIS PROGRAM SEGMENT CALCULATES THE 300- TO 500-MB AVERAGE WIND SPEED AND
C  DIRECTION
      DO 580 JJJ=20,30,2
       IF (WS(JJJ) .EQ. 99.9) GO TO 575
        RRRWD = RWD(JJJ)/57.296
        XMID = XMID +RWS(JJJ)*COS (RRRWD)
        YMID = YMID +RWS(JJJ)*SIN(RRRWD)
        GO TO 580
  575    JJJJ=JJJJ+1
  580   CONTINUE
      IF (JJJJ.EQ. 6) GO TO 590
      XAVMID = XMID/(6.-FLOAT(JJJJ))
      YAVMID = YMID/(6.-FLOAT(JJJJ))
      AVMSPD = SQRT(XAVMID **2+ YAVMID**2)
      Q = YAVMID/XAVMID
      AVMDIR = ATAN(Q)*57.296
      IF (XAVMID.GE.0.) GO TO 585
      AVMDIR = AVMDIR +180.
  585 IF ( AVMDIR .LT.0.) AVMDIR = AVMDIR +360.
      IF ( AVMDIR .GT. 360.) AVMDIR = AVMDIR-360.
      GO TO 600
  590 AVMSPD = -1.
```

```
      AVMDIR = -1.
C
C*****************************************************************************
C
C  CALCULATE SHEAR INDEX
C
  600 IC25C = 0
      F = 1.
      IXC25C = 0
      DO 665 JJK=III,IIIQ,2
        IF (CWS (JJK) .LT.0.) GO TO 625
        DIFF = CWS(JJK) -AVRWS
        ABC2 = .25*AVRWS
        IF (ABS(DIFF).LE. ABC2) GO TO 635
  625   F = 0.
        GO TO 665
  635 IF ( F .EQ. 0.) GO TO 640
        IC25C = IC25C +1
        GO TO 650
  640 IC25C =1
  650 IF ( IC25C .GT. IXC25C) IXC25C = IC25C
        F = 1.
        GO TO 665
  665   CONTINUE
      IF ( IXC25C .GT. INDSHR) INDSHR = IXC25C
      IF ( IXC25C .EQ. 0) GO TO 670
      GO TO 680
  670 IF (III.EQ. 1 .AND. K.EQ.1 .AND. L.EQ.1) GO TO 690
      GO TO 699
  680 IZERO = 1
      MM = ISAVE(IXC25C)
      MSS25 (IXC25C,MM) = IHUNPR
      MSD25 (IXC25C,MM) = IDEVIT
      DEV25 (IXC25C,MM) = DIR
      SRWS25 (IXC25C,MM) = AVRWS
      SRWD25 (IXC25C,MM) = AVRWD
      SS25(IXC25C,MM) = SS
      SD25 (IXC25C,MM) =SD
      DIRMID (IXC25C,MM) = AVMDIR
      SPDMID(IXC25C,MM) = AVMSPD
      ISAVE(IXC25C) = ISAVE(IXC25C) +1
      GO TO 699
  690 IZERO =0
      ISAVES = IHUNPR
      ISAVED = IDEVIT
      SAVEDV = DIR
      SAVEWS = AVRWS
      SAVEWD = AVRWD
      SAVES =SS
      SAVED= SD
      SAVEMD = AVMDIR
      SAVEMS = AVMSPD
  699 CONTINUE
C
C*****************************************************************************
C   CALCULATE ENERGY-SHEAR INDEX
C
C
      ESI = 4. -FLOAT (INDSHR)/2.+2.*EI
      IF (IZERO.EQ.0) GO TO 920
      DO 820 I =1,11
        IF ( ISAVE(I).EQ. 1) GO TO 910
        MMM= ISAVE (I)-1
C
C   OUTPUT RESULTS
C
```

```
C
      WRITE(6,1100)HEIGHT(100),PRESH(100),HEIGHT(0)
1100  FORMAT(' ','HEIGHT OF C B',F10.2,5X,'PRESSURE OF C B',F10.2,5X,
     1'850 MB HEIGHT',F10.2)
        WRITE (6,1110) I
 1110 FORMAT (//,33X,64HTHE FOLLOWING STORM SPEEDS AND DIRECTIONS GAVE A
     1SHEAR INDEX OF  ,I1,//)
        WRITE (6,1112)
 1112   FORMAT (28X,'STORM  SPEED',2X,15HSTORM DIRECTION,3X,3HDEV,6X,
     1 16HSURF-850 AVERAGE,8X,15H550-300 AVERAGE )
        WRITE (6,1114) (MSS25(I,J),SS25(I,J),MSD25(I,J),SD25(I,J),DEV25
     1(I,J),SRWS25(I,J),SRWD25(I,J),SPDM1D(I,J),DIRM1D(I,J),J=1,MMM)
 1114   FORMAT (28X,I2,1X,F5.2,4H MPS,3X,I2,1X,F6.2,4H DEG,3X,A5,3X,
     1F5.2,4H MPS,1X,F6.2,4H DEG,3X,F6.2,4H MPS,1X,F6.2,4H DEG)
        GO TO 820
  910   WRITE (6,1116) I
 1116   FORMAT (//,31X,' THERE WERE NO STORM SPEEDS AND DIRECTIONS THAT
     1GAVE A SHEAR INDEX OF',I1)
  820   CONTINUE
        GO TO 930
  920 WRITE (6,1118)
 1118 FORMAT (//,48X,36HTHIS SOUNDING HAD A SHEAR INDEX OF 0,//)
      WRITE (6,1112)
      WRITE (6,1114) ISAVES,SAVES,ISAVED,SAVED,SAVEDV,SAVEWS,SAVEWD,
     1 SAVEHD,SAVEHS
  930 WRITE (6,1120) EI,INDSHR,ESI
 1120 FORMAT (//,47X,5HEI=  ,F6.2,7H, SI = ,I1,12H, AND ESI = ,F6.2//)
      GO TO 1225
 1224 WRITE (6,6220) III,K,L,LLM,THWD,THWS,SINSS
 6220 FORMAT (4I6,3E15.7)
 1225 GO TO 100
      END
```

APPENDIX B

GENERAL WEATHER CONDITIONS

A tornado watch was issued for an area extending from central Tennessee into West Virginia at 1800 GMT 24 April. Severe thunderstorms and tornados occurred in northwest Tennessee, as a squall line moved into that region from Missouri. At this time, radiosonde stations in Nashville, Tennessee, and Marshall Space Flight Center, Huntsville, Alabama, recorded the highest wind speeds in the network at the 850-mb level.

By 2100 GMT, a strong squall line had formed over central Tennessee into western West Virginia. The cyclone in central Kansas continued to intensity and moved southeastward into northern Oklahoma with severe thunderstorms actively developing rapidly along the cold front. At the 200-mb level, high-speed winds extended from eastern Texas, across northern Louisiana, into Tennessee, Virginia, and West Virginia. Highest speeds were recorded at Nashville and Huntington. In the upper atmosphere the two jets had further diverged, moving into the northern tier of states and into central Texas and southern Louisiana, respectively.

Activity over the Appalachians had weakened by 0000 GMT 25 April. The severe squall and tornado watch area was extended into southwest Missouri as the frontal system moved slowly eastward. Severe thunderstorms and tornados occurred over Oklahoma and southwestern Missouri.

By 0600 GMT, the cyclone had moved eastward into Kentucky, as the severe squall line grew in both intensity and length. Severe thunderstorms and tornados were occurring in eastern Arkansas and western Tennessee. Warm air was flowing northeastward from the Gulf in this area at the 850-mb level. At the 200-mb level, flow was strongly turbulent over the west Tennessee-west Kentucky region.

APPENDIX C

UNUSUAL SEVERE WEATHER PHENOMENA DURING EXPERIMENTS [7]

1. April 24 2400 GMT, Grove County, Kansas: hail 2-in.-diam (tennis ball), $50,000 to $500,000.
2. April 24 2315 GMT, Wewoka, Seminole County, Oklahoma: hail 3-in.-diam (baseball), $50,000 to $500,000, thunderstorm $\vec{V}$ = northeastern, 3 mi/8 mi.
3. April 24 2325 GMT, Stilwell, Adair County, Oklahoma: hail 20 min, $50,000 to $500,000.
4. April 24 2400 GMT, Cotton County, Oklahoma: hail 1-in.-diam, 2-ft-deep, $50,000 to $500,000, thunderstorm $\vec{V}$ = east, 3 mi/20 mi.
5. April 24 2400 GMT, Craig and Ottawa Counties, Oklahoma: tornado $\vec{V}$ = east, 5 mi southwest Miami, $62,000 to $500,000,
6. April 24 1100 GMT, Nixa, Christian County, Missouri: thunderstorm $\vec{V}$ = southeast, two tornados (small), one east HW 65 and north Rt. 66, second Twin Acres.
7. April 25 0040 GMT, Newton County, Missouri: tornado $\vec{V}$ = east, Rt. 60, south Neosho, $105,000, 400 yd $\leftrightarrow$ 100 yd/9 mi.
8. April 24 2400 GMT, Pettis County, Missouri: hail 1-in.-diam, 2- to 3-ft-deep, $50,000 to $500,000.
9. April 25 0200 GMT, St. Louis, St. Louis County, Missouri: hail 1-in.-diam (golf ball), thunderstorms.

10. April 25 0200 GMT, Cedarville, Crawford County, Arkansas: funnel cloud $\vec{V}$ = northeast.
11. April 25 0549 GMT, Conway, Faulkner County, Arkansas: funnel cloud $\vec{V}$ = east.
12. April 25 0500-0555 GMT, Waldron, Scott County, Arkansas: thunderstorm, severe lightning.
13. April 25 0608 GMT, Walnut Ridge, Lawrence, County, Arkansas: funnel cloud $\vec{V}$ = east.
14. April 25 0630 GMT, Cotton Plant, Woodruff County, Arkansas: funnel cloud $\vec{V}$ = east.
15. April 25 0637 GMT, Forrest City, St. Francis County, Arkansas: funnel cloud $\vec{V}$ = east.
16. April 25 0620 GMT, Craighead County, Arkansas: line of thunderstorms $\vec{V}$ = southeast, wind, $50,000 to $500,000.
17. April 25 0645 GMT, Turrell, Crittenden County, Arkansas: tornado $\vec{V}$ = southeast, 40 yd/0.1 mi.
18. April 25 0800-1200 GMT, southeastern Illinois: rain, earthen dam collapse.
19. April 25 0200-0800 GMT, southern one-third of Illinois: hail, thunderstorm, $5,000 to $50,000.
20. April 24-25, southern Indiana: heavy rain, $500,000 to $5,000,000.
21. April 24-25, west and south central Kentucky: thunderstorms, rain, flooding.
22. April 25 1030 GMT, Water Valley, Itawaba County, Mississippi: winds.

23. April 24 1000 GMT, northern Alabama: thunderstorms $\vec{V}$ = east, tornado, $50,000 to $500,000.
24. April 24 1630 GMT, Weakley County, Tennessee: tornado, 200 yd/0.5 mi.
25. April 24 2000 GMT, Macon County, Tennessee: winds, $5,000 to $50,000.
26. April 24 2230 GMT, Cumberland County, Tennessee: tornado, 440 yd/1.5 mi., $50,000 to $500,000.
27. April 25 0200 GMT, Tipton County, Tennessee: tornado, 400 yd/6 mi., $5,000 to $50,000.
28. April 25 0720 GMT, Crockett County, Tennessee: tornado, Cairo, Nance, Quincy communities, 440 yd/11 mi., $50,000 to $500,000.
29. April 25 0740 GMT, Humboldt and Gibson Counties, Tennessee: winds, $50,000 to $500,000.
30. April 25 0800 GMT, Carroll County, Tennessee: winds, $5,000 to $50,000.